Photochemical & Photobiological Sciences (2022) 21:1309–1331
https://doi.org/10.1007/s43630-022-00186-3

REVIEWS

Spin-flip luminescence

Winald Robert Kitzmann[1] · **Johannes Moll**[1] · **Katja Heinze**[1]

Received: 23 December 2021 / Accepted: 1 February 2022 / Published online: 5 March 2022
© The Author(s) 2022

Abstract

In molecular photochemistry, charge-transfer emission is well understood and widely exploited. In contrast, luminescent metal-centered transitions only came into focus in recent years. This gave rise to strongly phosphorescent Cr^{III} complexes with a d^3 electronic configuration featuring luminescent metal-centered excited states which are characterized by the flip of a single spin. These so-called spin-flip emitters possess unique properties and require different design strategies than traditional charge-transfer phosphors. In this review, we give a brief introduction to ligand field theory as a framework to understand this phenomenon and outline prerequisites for efficient spin-flip emission including ligand field strength, symmetry, intersystem crossing and common deactivation pathways using Cr^{III} complexes as instructive examples. The recent progress and associated challenges of tuning the energies of emissive excited states and of emerging applications of the unique photophysical properties of spin-flip emitters are discussed. Finally, we summarize the current state-of-the-art and challenges of spin-flip emitters beyond Cr^{III} with d^2, d^3, d^4 and d^8 electronic configuration, where we mainly cover pseudooctahedral molecular complexes of V, Mo, W, Mn, Re and Ni, and highlight possible future research opportunities.

Graphical abstract

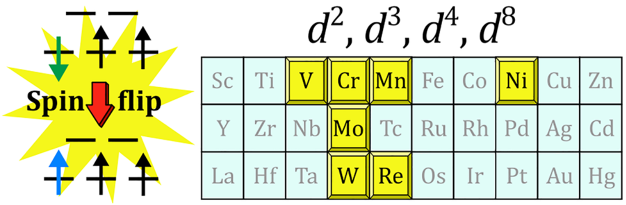

Keywords Transition metal complex · Photochemistry · Excited states · Ligand field theory · Spin-flip phosphorescence · Intersystem crossing

1 Introduction and scope of the review

Photoactive complexes are both fundamentally interesting and highly valuable in many applications, e.g., optical devices, catalysis and biomedicine [1–4]. Traditionally there is an excessive reliance on compounds containing precious transition metal ions like Ru^{II}, Ir^{III}, Os^{II} or Pt^{II} due to their favorably high intrinsic ligand field splitting and strong spin–orbit coupling (SOC) [5–9]. In most cases, the emissive states are of charge transfer (CT) character, be it metal-to-ligand (MLCT), ligand-to-metal (LMCT), ligand-to-ligand (LL'CT) or intra-ligand charge transfer (ILCT), while metal-centered (MC) states are often non-emissive and facilitate non-radiative deactivation [10, 11].

Most prominently, this occurs in Fe^{II} complexes where efficient relaxation via low-energy MC states had precluded long MLCT lifetimes and phosphorescence for a long time [12–20]. An octahedral Fe^{II} complex with tridentate N^N^N ligands showed a $^{3/5}$MC lifetime of > 1.6 ns and sensitized $^1O_2$ [15] and an iron(II) complex with a hexadentate tren(py)$_3$ ligand reduces quinones by photoinduced electron

---

Winald Robert Kitzmann
Kitzmann@Uni-Mainz.de

Katja Heinze
Katja.Heinze@Uni-Mainz.de

[1] Department of Chemistry, Johannes Gutenberg University Mainz, Duesbergweg 10–14, Mainz, Germany

transfer from its ^{5}MC state (tren(py)$_3$ = *tris*(2-pyridyl-methyliminoethyl)amine) [18]. An excited ^{3}CT state lifetime of 3 ns was achieved by an iron(II) complex with strongly covalent Fe–N$_{\text{amido}}$ bonds due to a high barrier for the ^{3}MC/^{3}CT interconversion [21]. Most recently, the first emissive mononuclear Fe$^{\text{II}}$ complex has been reported [22]. It shows NIR-II luminescence in the range of 1030–1600 nm originating from a ^{3}MLCT state with a lifetime of 1 ns in benzene solution at room temperature.

Rare examples of d^6 complexes showing luminescent ^{3}MC states were presented with $[\text{Co}^{\text{III}}(\text{CN})_6]^{3-}$ and more recently with a hexacarbene Co$^{\text{III}}$ complex [23, 24]. The strongly σ-donating ligands imposed a very high ligand field splitting. This raised the energy of MC states so they can act as long-lived emissive excited states [24].

A fundamentally different type of phosphorescence from MC states appears in octahedral d^3–Cr$^{\text{III}}$ complexes. Instead of interconfigurational states with occupied antibonding orbitals, associated emissive MC states feature the same electronic configuration as the ground state $(t_{2g})^3$, but differ by a single flipped electron spin. Hence, this luminescence from intraconfigurational states was named 'spin-flip emission'. Although Cr$^{\text{III}}$ complexes have been known for many years, a conceptual breakthrough toward intense spin-flip emission led to an increased interest in the past six years [11, 25–29].

Beyond the d^3 electronic configuration, spin-flip emission is also conceivable in octahedral d^2, d^4 and d^8 complexes, but examples are much less prevalent in the literature than for d^3 complexes. In this review, we outline the theoretical frame required to understand spin-flip luminescence with respect to ligand field theory, symmetry, intersystem crossing (ISC) and relaxation pathways using various well-described Cr$^{\text{III}}$ complexes. We also show how emission energies can be tuned in these systems over a range of 5800 cm^{-1}, and which applications exploit their unique excited state properties. Finally, we summarize the advances of the field with special emphasis on the often-undervalued central ions V$^{\text{II}}$, V$^{\text{III}}$, Cr$^{\text{IV}}$, Mo$^{\text{III}}$, W$^{\text{III}}$, Mn$^{\text{IV}}$, Re$^{\text{IV}}$ and Ni$^{\text{II}}$. While spin-flip emission has been observed in many solids doped with suitable transition metal ions [30–46] and many lanthanide complexes show emissive metal-centered *ff*-transitions [47–49], this review focuses on mononuclear molecular systems with *d*-block transition metal ions.

2 Implications from ligand field theory

Ligand field theory is a powerful tool to understand and design spin-flip emitters. In an octahedral ligand field the five degenerate *d*-orbitals split into two sets, three lower t_{2g} and two higher e_g* orbitals (O_h notation), which differ in energy by the ligand field splitting Δ_O [50, 51]. The ligand field concomitantly leads to splitting of the atomic terms of the central metal forming ligand field terms of different symmetries. The energies of these terms in dependence of Δ_O are visualized in Tanabe-Sugano (TS) diagrams and depend on Δ_O as well as the Racah parameters *B* and *C* (Fig. 1) [52, 53]. While both *B* and *C* describe the interelectronic repulsion, the parameter *C* only affects the energies of states with multiplicities lower than the maximum for a given electronic configuration (for example those of the doublet states in d^3 ions) [54]. The relative state energies in a TS diagram depend on the ratio *C*/*B* which is often arbitrarily set to 4.0 but in reality varies between complexes [55]. Figure 1 shows the TS diagrams for octahedral d^2, d^3, d^4 and d^8 complexes [52, 53]. These electronic configurations feature a set of intraconfigurational states with low energy at high Δ_O (e.g., ^{2}E and ^{2}T$_1$ for d^3, O_h notation with *g*/*u* omitted). These intraconfigurational states possess a nearly unchanged electron distribution compared to the ground state, e.g., $(t_{2g})^3$ for the ^{4}A$_2$ state in d^3. This has two consequences: their energy is essentially ligand field-independent (Eqs. 1 and 2) and they show a geometry close to the ground-state geometry (nested states, ^{2}E/^{2}T$_1$ states in Fig. 2, weak coupling limit). In contrast, the occupation of orbitals of different energies in interconfigurational states like the ^{4}T$_2$ and ^{4}T$_1$ states in d^3 ions (Eqs. 3 and 4) or charge-transfer states results in horizontally shifted and broad potential wells (^{4}T$_2$ state in Fig. 2, strong coupling limit). Consequently, this shift can lead to enhanced non-radiative relaxation to the ground state and broader emission bands, while spin-flip emission is typically very sharp [56].

In general, the transition energies from the ground state to excited MC states with the highest possible multiplicity like ^{4}T$_2$ and ^{4}T$_1$ in the d^3 electron configuration can be described with Δ_O and the Racah parameter *B* (Eqs. 3 and 4), while those with lower multiplicity like the ^{2}E and ^{2}T$_1$ states also require the Racah parameter *C* (Eqs. 1 and 2) [50, 57]. It should be noted that Eqs. 1 and 2 were generated by assuming *C*/*B* = 4 for the calculation of the configurational interaction terms as multiples of B^2/Δ_O [50, 57]. For exact solutions, the reader is referred to Ref. [58].

$$E(^2E) - E(^4A_2) \approx 9B + 3C - 50\left(\frac{B^2}{\Delta_O}\right) \tag{1}$$

$$E(^2T_1) - E(^4A_2) \approx 9B + 3C - 24\left(\frac{B^2}{\Delta_O}\right) \tag{2}$$

$$E(^4T_2) - E(^4A_2) = \Delta_O \tag{3}$$

Fig. 1 Tanabe-Sugano (TS) diagrams of **a** d^2, **b** d^3, **c** d^4 and **d** d^8 transition metal ions in octahedral fields with $C/B = 4$ [50, 52, 53, 58]. Important crossing points are marked with circles. Exemplary intraconfigurational microstates relevant for spin-flip emission and detrimental interconfigurational microstates were empirically derived from complete active space self-consistent field (CASSCF) calculations of perfectly octahedral model complexes $[MH_6]^{n-}$ ($M = V^{III}$, Cr^{III}, Mo^{II}, Ni^{II}; see Supporting Information for computational details). Dotted lines in the microstates indicate strong mixing ▸

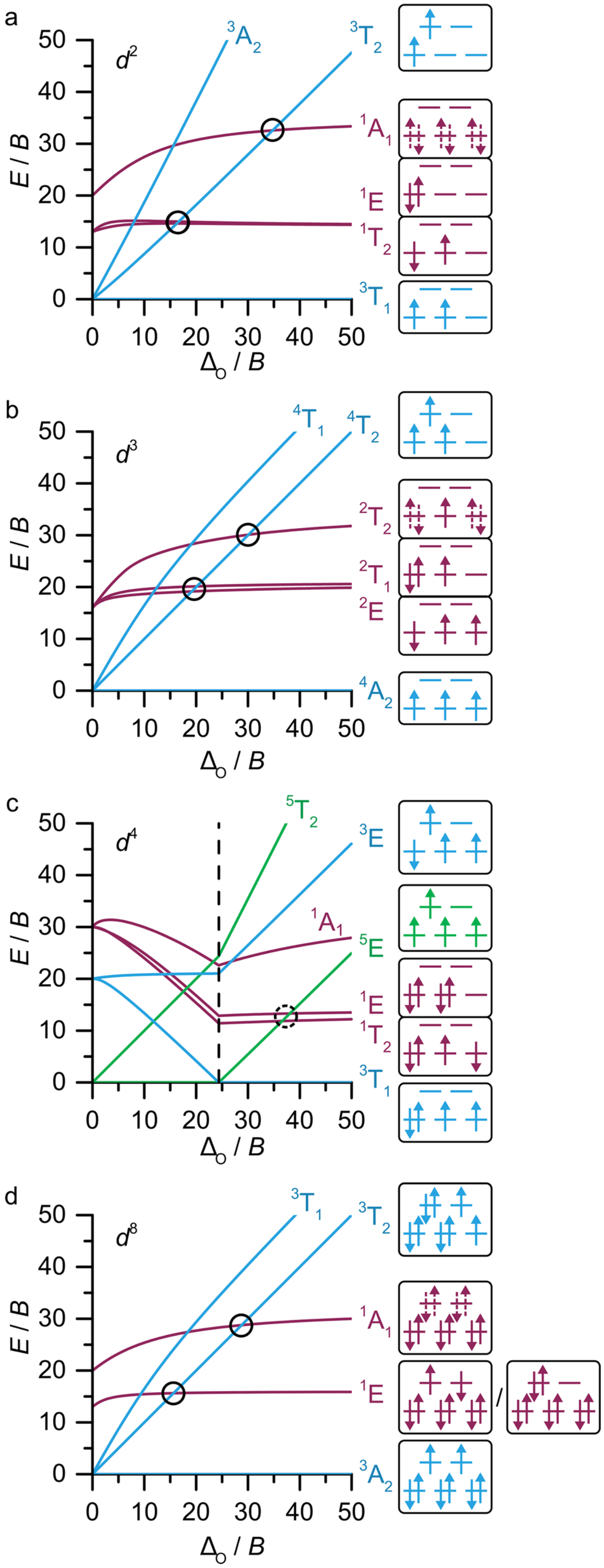

$$E\left({}^4T_1\right) - E\left({}^4A_2\right) = 1.5\Delta_O + 7.5B - 0.5\sqrt{225B^2 + \left(\Delta_O\right)^2 - 18\Delta_O B}. \tag{4}$$

As discussed in more detail below, tuning of the excited MC state energies via the ligand field strength Δ_O is well understood and heavily exploited in the design of spin-flip emitters (see Sect. 3.1). Yet designing systems with tailored Racah parameters B and C and thus spin-flip phosphorescence energy is difficult (see Sect. 4). Similarly, to achieve MLCT emission from Fe^{II} complexes, many studies focused on imposing a high ligand field splitting Δ_O to raise the MC states as potential deactivating states above the MLCT states [10, 19, 59]. Recently, a new design strategy featured increased metal–ligand covalency leading to decreased interelectronic repulsion, which counteracted the lower Δ_O and yielded an excited state lifetime of 3 ns of a pseudo-octahedral iron(II) complex [21].

While ligand field theory and the derived TS diagrams are useful to identify certain trends, they come with some limitations: (1) The diagrams refer to a perfectly octahedral coordination geometry. (2) Spin–orbit coupling (SOC) and hence mixing of states with different multiplicity is neglected. (3) Both a lower symmetry of the ground state and SOC lead to splitting of degenerate ligand field terms. (4) TS diagrams reflect the state energies at the ground-state geometry (Franck–Condon state) and neglect excited state energy lowering by excited state distortion. (5) CT states are not considered but can sometimes play an important role in the photodynamics of spin-flip emitters as discussed below.

3 Prerequisites for strong spin-flip emission

In this section, parameters influencing spin-flip emission and excited state relaxation pathways are discussed using d^3–Cr^{III} complexes as instructive and well-explored examples.

3.1 Strong ligand field splitting to avoid relaxation via MC states

Spin-flip phosphorescence is favored when the spin-flip states are the lowest energy excited states, even though it is a spin-forbidden process. As discussed in the previous

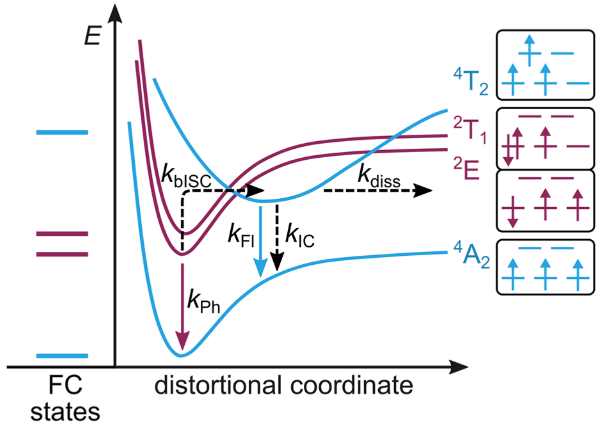

Fig. 2 Schematic potential energy diagram of an octahedral d^3 transition metal complex with Δ_O beyond the first quartet-doublet crossing point $^4T_2$–^2E in the TS diagram (Fig. 1b) and energies of the Franck–Condon (FC) states. Radiative (phosphorescence k_{Ph} and fluorescence k_{Fl}) and non-radiative decay pathways (back-intersystem crossing k_{bISC}, dissociation k_{diss} and internal conversion k_{IC}) and exemplary microstates of the relevant states are depicted [56]

section, this energy level ordering requires a high ligand field splitting Δ_O. In case of Cr^{III} this necessitates strongly σ-donating ligands, since the 3*d* orbitals possess a rather contracted radial distribution function (primogenic effect) [60, 61]. This limits overlap with ligand orbitals, which is referred to as a low intrinsic ligand field strength [62]. For d^3 ions in an octahedral ligand field, the $^4T_2$ state rises above the ^2E and $^2T_1$ states with increasing Δ_O (Fig. 1b). For Cr^{III} ions this could not be fully achieved using traditional ligands like en or tpy with their homoleptic complexes showing only weak spin-flip phosphorescence ([Cr^{III}(en)$_3$]$^{3+}$ **Cr1^{3+}**: $\Phi = 0.0062\%$, [Cr^{III}(tpy)$_2$]$^{3+}$ **Cr2^{3+}**: $\Phi < 0.001\%$; en = 1,2-ethylenediamine, tpy = 2,2';6',2''-terpyridine; Scheme 1, Table 1) [63, 64]. These ligands form five-membered chelate rings with the metal ion which leads to substantial deviation of 7°–11° from perfectly octahedral geometry (∠(N–Cr–N) = 90° or 180°) and a weak σ-orbital overlap [56, 65]. As a result, **Cr1^{3+}** and **Cr2^{3+}** only reach the first $^4T_2$–^2E crossing point in the TS diagram (Fig. 1b). Weakly luminescent Cr^{III}(acac)$_3$ **Cr3** serves to discuss the effects of a small Δ_O (acac$^-$ = acetylacetonato, Scheme 1, Table 1).

For **Cr3**, quantum chemical calculations placed the $^4T_2$ state close to the $^2T_1$ state in the FC region, i.e., close to the first quartet-doublet crossing point $^4T_2$–^2E in the TS diagram (Fig. 1b), leading to a high density of states. Furthermore, large SOC constants of 100–170 cm^{-1} were calculated between the $^4T_2$ and $^2T_1$ states [66]. This is in agreement with El Sayed' rule stating that SOC between two states is large when a change in spin multiplicity is accompanied by a change in orbital angular momentum. The orbital character changes during ISC from the $^4T_2$ state with $(t_{2g})^2(e_g{*})^1$ to the $^2T_1$ state with $(t_{2g})^3(e_g{*})^0$ electron configuration [67]. Consequently, wavepacket simulations predicted an ultrafast $^4T_2 \rightarrow {}^2T_1$ ISC for **Cr3** [66]. In fact, fs-transient absorption studies with ligand field excitation revealed ISC with $\tau_{ISC} < 100$ fs, that competes with vibrational cooling (VC) in the $^4T_2$ state. An experimental time constant of $\tau = 1.1(1)$ ps was assigned to VC in the doublet states state [68].

Apart from facilitating ISC, a small energy separation between $^4T_2$ and $^2E/^2T_1$ states enables back-intersystem crossing (bISC) from the doublet manifold to the $^4T_2$ state [69]. This results in low phosphorescence quantum yields and a low photostability of the complexes, since the $^4T_2$ state with its $(t_{2g})^2(e_g{*})^1$ electronic configuration is Jahn–Teller distorted and potentially dissociative [25, 70, 71].

A conceptual breakthrough was achieved with [Cr^{III}(ddpd)$_2$]$^{3+}$ **Cr4^{3+}** (ddpd = *N*,*N*'-dimethyl-*N*,*N*'-dipyridin-2-ylpyridine-2,6-diamine, Scheme 1, Table 1) showing a very strong and long-lived dual emission in the near-infrared (NIR, 738 and 775 nm, $\Phi = 11\%$, $\tau = 899$ µs) after $^4A_2 \rightarrow {}^4$LMCT or $^4A_2 \rightarrow {}^4T_2$ excitation at 435 nm [25]. In **Cr4^{3+}**, the tridentate tpy-like ligand was formally expanded by NMe bridges leading to six-membered chelate rings with almost perfectly octahedral coordination with respect to the [CrN$_6$] coordination polyhedron. The resulting very strong ligand field raised the $^4T_2$ state to the level of the $^2T_2$ state, close to the second quartet-doublet crossing point $^4T_2$–$^2T_2$ in the TS diagram (Fig. 1b) [72]. At this crossing point with roughly degenerate $^4T_2$ and $^2T_2$ states at the FC geometry, ISC from the $^4T_2$ state to the $^2T_2$ state might be facilitated by a high density of doublet states [67] as well as a large SOC constant of 42 cm^{-1} between the $^4T_2(1)$ and $^2T_2(2)$ states as calculated using multi-reference methods [73]. Furthermore, the internal conversion (IC) $^2T_2 \rightarrow {}^2E/^2T_1$ might be faster than the bISC process $^2T_2 \rightarrow {}^4T_2$ resulting in efficient population of the emissive $^2E/^2T_1$ states. In fact, after excitation to the $^4T_2$ states, fast ISC and vibrational cooling (VC) populate the thermalized doublet states $^2E/^2T_1$ within $\tau = 3.5$ ps [74]. The significant ^2E–$^4T_2$ energy gap of the relaxed excited states of 7100 cm^{-1} effectively prevents bISC and enables radiative relaxation (k_{Ph}) to the ground state [25]. **Cr4^{3+}** is called '*Molecular Ruby*' because of its optical properties reminiscent of the gemstone ruby (Al$_2$O$_3$:Cr^{3+}) [25]. The nickname was recently adapted for the emerging class of strongly luminescent Cr^{III} complexes [25, 28, 73].

3.2 Relaxation via CT states

Aside from interconfigurational MC states, CT states need to be considered as relaxation pathways in spin-flip emitters as well. Complexes of V^{II}, Cr^{III} and Mn^{IV} all feature a d^3 electronic configuration. However, due to the different oxidation state of the central metal ions, low-energy MLCT and LMCT states can arise in V^{II} and Mn^{IV} complexes,

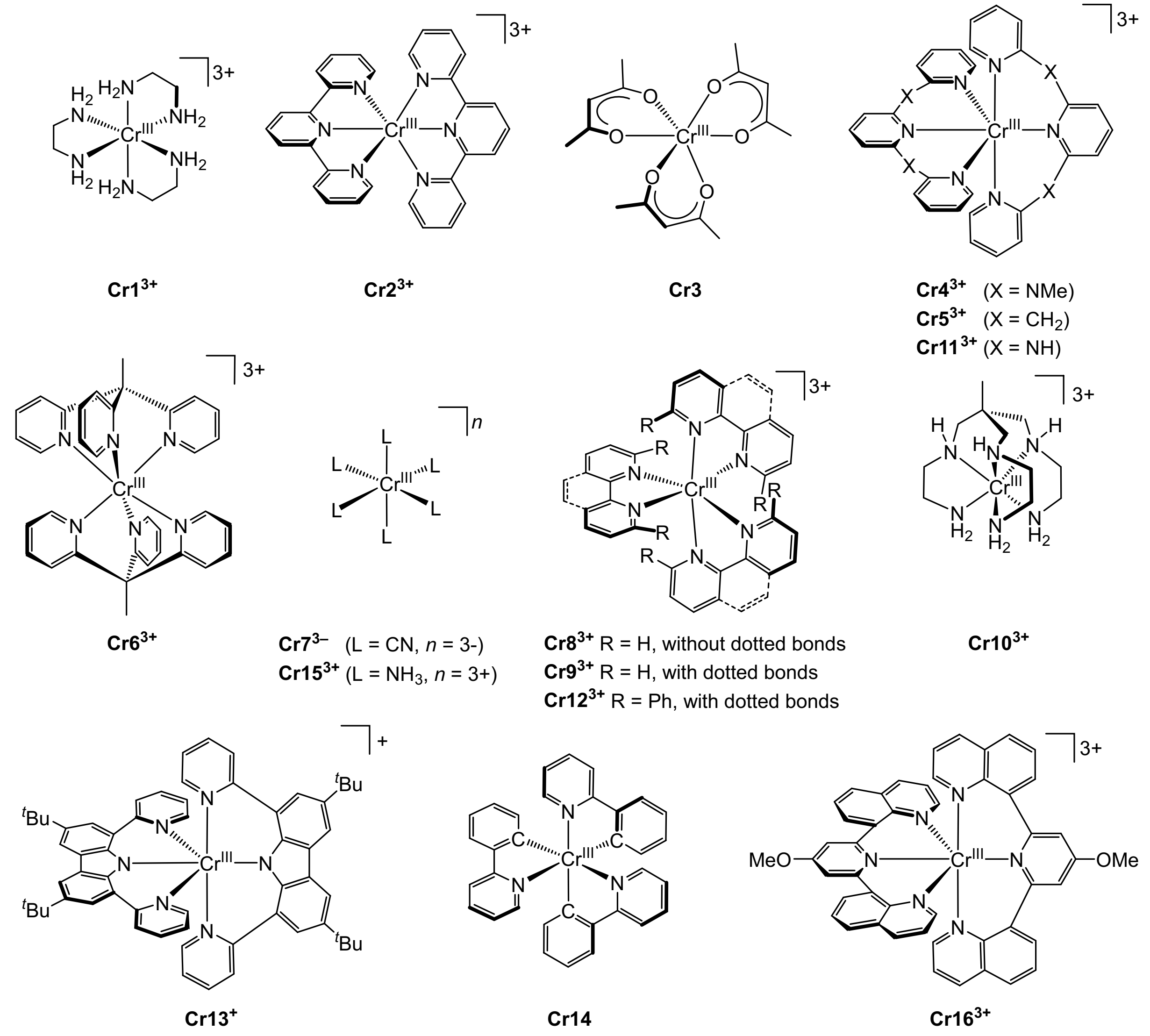

Scheme 1 Cr^{III} complexes discussed in this review

respectively (see below for more details) [42, 89]. For Cr^{III}, CT states are of relatively high energy (e.g., the superposition of ^{4}LMCT and $^4T_2$ absorption bands at 435 nm in **Cr4**$^{3+}$ [25]) or they can be avoided altogether in the region of the $^4T_2$ absorption as demonstrated with $[Cr^{III}(bpmp)_2]^{3+}$ **Cr5**$^{3+}$ and $[Cr^{III}(tpe)_2]^{3+}$ **Cr6**$^{3+}$ (bpmp = 2,6-bis(2-pyridylmethyl) pyridine, tpe = 1,1,1-tris(pyrid-2-yl)ethane; Scheme 1, Table 1) [73, 78]. Since low-energy CT states or their admixture to spin-flip states as in $[V^{II}(bpy)_3]^{2+}$ (bpy = 2,2'-bipyridine) may act as relaxation pathways for long-lived spin-flip states [89], the relative energies of ligand and central metal orbitals need to be taken into account when designing ligands for spin-flip emitters.

3.3 Symmetry

The intraconfigurational spin-flip transition is governed by two selection rules: it is a spin-forbidden process and additionally Laporte's rule applies, which forbids electronic transitions between wave functions of the same parity [90]. In centrosymmetric $[Cr^{III}(CN)_6]^{3-}$ **Cr7**$^{3-}$ the combination of Laporte and spin selection rules leads to very long-lived emission (τ = 3.45 ms) in frozen solution at 77 K with a low radiative rate constant of k_{Ph} = 25 s^{-1} (Scheme 1, Table 1) [80, 91]. Irradiation of **Cr7**$^{3-}$ in aqueous solution can lead to ligand substitution [70]. The tripodal chelating ligand tpe imposes inversion symmetry on $[Cr^{III}(tpe)_2]^{3+}$ **Cr6**$^{3+}$ (Scheme 1, Table 1) resulting in a record lifetime of 4.5 ms in $DClO_4/D_2O$ at room temperature while retaining a high phosphorescence quantum yield of 8.2% [78]. Due to the

Table 1 Optical properties of luminescent Cr^{III} complexes with phosphorescence emission maximum λ_{max}, luminescence lifetime τ and quantum yield Φ measured in the absence of oxygen if not stated otherwise

Number	Complex	Medium	λ_{max}/nm	τ/µs	Φ/%	References
Cr1^{3+}	$[Cr^{III}(en)_3]^{3+}$	H_2O	670	1.85 ^{a}	0.0062	[63, 75]
Cr2^{3+}	$[Cr^{III}(tpy)_2]^{3+}$	MeCN	770	0.14	$<0.001^{b}$	[64, 76]
Cr3	$Cr^{III}(acac)_3$	MeOH/EtOH (77 K)	785	431	–	[77]
Cr4^{3+}	$[Cr^{III}(ddpd)]_2]^{3+}$	H_2O	738, 775	889	11.0	[25]
		D_2O	738, 775	1164	14.2	[79]
$[D_{18}]$-**Cr4**$^{3+}$	$[Cr^{III}([D_9]\text{-ddpd})]_2]^{3+}$	CD_3CN	738, 775	2300	30.1	[79]
Cr5^{3+}	$[Cr^{III}(bpmp)_2]^{3+}$	$D_2O/DClO_4$	709	1800	20.0	[73]
$[D_4]$-**Cr5**$^{3+}$	$[Cr^{III}([D_2]\text{-bpmp})_2]^{3+}$	$D_2O/DClO_4$	709	2500	24.6	[73]
Cr6^{3+}	$[Cr^{III}(tpe)_2]^{3+}$	H_2O	748	–	3.2	[78]
		$H_2O/HClO_4$	748	2800	5.4	[78]
		$D_2O/DClO_4$	748	4500	8.2	[78]
Cr7^{3-}	$[Cr^{III}(CN)_6]^{3-}$	H_2O	820	0.14^{a}	$<5\cdot10^{-6}$	[63]
		Rigid glass^{c} (77 K)	–	3450^{c}	–	[80]
Cr8^{3+}	$[Cr^{III}(bpy)_3]^{3+}$	H_2O	727	74	0.089^{a}	[63, 81]
		1 M $HCl_{(aq)}$	729	69	0.25	[82]
Cr9^{3+}	$[Cr^{III}(phen)_3]^{3+}$	H_2O	689, 726	356	0.15	[27, 81, 83]
		1 M $HCl_{(aq)}$	730	304	1.2	[82]
Cr10^{3+}	$[Cr^{III}(sen)]^{3+}$	H_2O/DMSO (77 K)	675	0.0001^{d}	–	[84]
Cr11^{+}	$[Cr^{III}(H_2tpda)_2]^{3+}$	MeCN	738, 782	770	8.8	[85]
Cr12^{3+}	$[Cr^{III}(Ph_2phen)_3]^{3+}$	1 M $HCl_{(aq)}$	744	304	3.0	[82]
		CH_3NO_2	750	441	–	[86]
		CH_3NO_2	750	13^{a}	–	[86]
Cr13^{+}	$[Cr^{III}(dpc)_2]^{+}$	MeCN (77 K)	1067	2.0^{e}	$<8.9\times10^{-4}$	[87]
Cr14	$Cr^{III}(ppy)_3$	2-MeTHF	910	9.5	0.03	[88]
		2-MeTHF (77 K)	890	48	–	[88]
Cr15^{3+}	$[Cr^{III}(NH_3)_6]^{3+}$	H_2O	667	2.2^{a}	0.0055^{a}	[63]
Cr16^{3+}	$[Cr^{III}(dqp^{OMe})_2]^{3+}$	H_2O	756	1350	17.0	[29]

[a] Measured in aerated solution

[b] Measured in water

[c] Measured either in MeOH/H_2O/ethylene glycol (2:1:1) or MeOH/EtOH (1:1)

[d] Extrapolated from temperature dependent lifetime measurements in glassy media at low temperatures

[e] Amplitude averaged lifetime of biexponential fit with $\tau_1 = 1.4$ µs (88%) and $\tau_2 = 6.3$ µs (12%)

inversion symmetry, the extinction coefficient for the $^4A_2 \rightarrow {}^4T_2$ transition is very low ($\varepsilon = 30$ M^{-1} cm^{-1}, Laporte forbidden), as is the radiative rate constant of the NIR phosphorescence ($k_{Ph} = 18$ s^{-1}, Laporte and spin-forbidden) [78]. On the other hand, the coordinating nitrogen atoms in the ddpd complex **Cr4**$^{3+}$ are arranged around a center of symmetry $[CrN_6]$ but the overall symmetry is lower due to the orientation of the pyridine rings (point group D_2). This allows for a faster radiative decay k_{Ph} and thus leads to a shorter lifetime of 899 µs [25]. Lower symmetry also lifts the degeneracy of the E and T states, which influences band shape and transition energy of the spin-flip luminescence [27, 72]. The radiative rate k_{Ph} increases by removing the center of inversion from **Cr6**$^{3+}$ to **Cr4**$^{3+}$ lifting Laporte's rule [78].

In addition, symmetry can also influence non-radiative relaxation pathways opened by geometric distortions. In tris(bidentate)chromium(III) complexes with D_3 or D_{3h} symmetry like $[Cr^{III}(bpy)_3]^{3+}$ **Cr8**$^{3+}$, a trigonal distortion of the coordination sphere in the long-lived excited states can lead to surface crossing of the excited doublet states with the ground state [84, 92]. This relaxation pathway limits the phosphorescence quantum yields with 0.15% obtained for $[Cr^{III}(phen)_3]^{3+}$ **Cr9**$^{3+}$ in water (phen = 1,10-phenanthroline, Scheme 1, Table 1) [93]. In 1 M aqueous HCl, the quantum yield is reported as 1.2% with $\tau = 304$ µs [82]. The pair $[Cr^{III}(en)_3]^{3+}$ **Cr1**$^{3+}$ and the trigonally distorted cage complex $[Cr^{III}(sen)]^{3+}$ **Cr10**$^{3+}$ displays an even stronger effect with a reduction of the excited state lifetimes from $\tau = 1.2$–1.85 µs to $\tau = 0.0001$ µs (sen = 4, 4', 4''-ethylidenetris(3-azabutane-1-amine); Scheme 1, Table 1) [63, 75, 84]. The hexadentate ligand in **Cr10**$^{3+}$ apparently enables efficient non-radiative relaxation pathways due to trigonal distortion which are unavailable in **Cr1**$^{3+}$.

3.4 Multi-phonon relaxation

The low energy of the doublet states in Cr^{III}-based spin-flip emitters (typically 12,800–15,000 cm^{-1}) [94] enables non-radiative decay via energy transfer to vibrational overtones of nearby X–H oscillators (X = C, N, O) [95]. This constitutes a major obstacle for efficient molecular emitters with organic ligands but not for oxidic materials such as ruby. By almost quantitative deuteration of the ligand in [Cr^{III}([D$_9$]-ddpd)$_2$]$^{3+}$ [D$_{18}$]-**Cr4**$^{3+}$, a record quantum yield of 30% could be achieved (Table 1) [79]. This effect is due to the lower energy of the C–D fundamental mode (≈2200 cm^{-1}) and its overtones compared to C–H vibrations (≈3000 cm^{-1}). To deactivate the excited doublet state in the deuterated *Molecular Ruby*, energy transfer to a higher vibrational overtone (v^6) with a lower $v_0 \rightarrow v_6$ extinction coefficient is necessary than with C–H oscillators ($v^4 + v^5$). In case of acetonitrile, solvent deuteration had a negligible effect, whereas τ and Φ of **Cr4**$^{3+}$ significantly increased from 898 to 1164 µs and from 11.0 to 14.2%, respectively, in D_2O instead of H_2O [79].

In [Cr^{III}(bpmp)$_2$]$^{3+}$ **Cr5**$^{3+}$ (Scheme 1, Table 1) with an emission maximum at 709 nm, selective α-deuteration of the ligand yielding [Cr^{III}([D$_2$]-bpmp)$_2$]$^{3+}$ [D$_4$]-**Cr5**$^{3+}$ increased the quantum yield and lifetime from 20 to 25% and from 1.8 to 2.5 ms, respectively (Table 1) [73]. Clearly, the C–H oscillators closest to the Cr^{III} center ($d \approx 3.0$ Å) affect the multiphonon energy transfer the most, while the more distant oscillators play only a minor role due to the d^{-6} dependence of the corresponding rate constant [95].

Due to the higher energy of the N–H vibrations (3400 cm^{-1}) and their different anharmonicity, multiphonon quenching is very pronounced in complexes like **Cr1**$^{3+}$, **Cr10**$^{3+}$ and [Cr^{III}(H$_2$tpda)$_2$]$^{3+}$ **Cr11**$^{3+}$ (H$_2$tpda = 2,6-bis(2-pyridylamino)pyridine; Scheme 1, Table 1). N–H/N–D exchange on the ligands increased quantum yields by factors of 2.2–25 [84, 85]. Again, multiphonon quenching strongly depends on the Cr···(H–X) distance d with N–H bonds in **Cr1**$^{3+}$ ($d = 2.48$ Å) being closer to the metal center than in **Cr11**$^{3+}$ ($d = 3.1$–3.8 Å) [65, 85].

3.5 Solvent effects and counter ions

Apart from deuteration effects discussed in the previous section, solvents, salt additives and the counter ions of the complexes can influence their photophysical properties.

In **Cr6**$^{3+}$, the phosphorescence quantum yield increased from 3.2% in H_2O to 4.2% and 5.4% in 0.1 M $NaClO_{4(aq)}$ and 0.1 M $HClO_{4(aq)}$, respectively. It was suggested that the perchlorate ions and the acid protect the charged complex from solvent molecules [78]. A similar effect was found for **Cr8**$^{3+}$, which possesses increased lifetimes in the presence of salts (e.g., $NaClO_4$) or acids in high concentrations (> 1 M). Here, the effect was rationalized by perchlorate ions filling the pockets between the bpy ligands in **Cr8**$^{3+}$ leading to a rigidification and thus inhibiting distortional non-radiative relaxation (see Sect. 3.3). The influence of the solvent is much less pronounced for **Cr9**$^{3+}$ ($\tau_{HClO4}/\tau_{H2O} \approx 2$) than for **Cr8**$^{3+}$ ($\tau_{HClO4}/\tau_{H2O} \approx 11$), probably since the phen ligand scaffold of **Cr9**$^{3+}$ is more rigid on its own [96]. In general, relatively high phosphorescence quantum yields were found for tris(bidentate)chromium(III) polypyridyl complexes like **Cr8**$^{3+}$ ($\Phi = 0.25\%$), **Cr9**$^{3+}$ ($\Phi = 1.2\%$) and [Cr^{III}(Ph$_2$phen)$_3$]$^{3+}$ **Cr12**$^{3+}$ ($\Phi = 3.0\%$) in 1 M $HCl_{(aq)}$ (Table 1, Scheme 1, Ph$_2$phen = 4,7-diphenyl-1,10-phenanthroline) [82]. For **Cr4**$^{3+}$, there was no effect on lifetime or quantum yield when using dilute $HClO_{4(aq)}$ instead of water [25, 78].

Absorption/emission profiles and lifetimes of the bpy complex **Cr8**$^{3+}$ remained unchanged in non-aqueous solvents like MeOH, MeCN, dimethylformamide (DMF) and ethylene glycol [96]. Yet, the $^4T_2 \rightarrow {}^2E$ ISC efficiency decreased in these solvents [97]. The emission lifetime of the cyanido complex **Cr7**$^{3-}$ correlated with solvent polarity [91], while the emission of the en complex **Cr1**$^{3+}$ remained unaffected by the presence of $MgCl_2$ up to 5.2 M [98].

Cr4[BF$_4$]$_3$ forms a contact ion pair with one [BF$_4$]$^-$ anion on average in acetonitrile solution, due to the high charge of the complex cation [99]. In fact, the counter ions of **Cr4**$^{3+}$ affect the phosphorescence lifetime and quantum yield [100]. In acetonitrile solution, Φ increased from 5.2% with chloride anions to 13.6% with tetrakis(3,5-bis(trifluoromethyl)phenyl)borate [BArF$_{24}$]$^-$. This change was attributed to reduced self-quenching when employing bulky anions. However, tetraphenylborate [BPh$_4$]$^-$ led to lower quantum yields of 9.2% likely due to the introduction of additional C–H oscillators close to the Cr^{III} center in contact ion pairs enabling multiphonon relaxation (see above). The counter ions affected lifetime and quantum yield in parallel. Thus, only the non-radiative relaxation pathways from the long-lived $^2E/^2T_1$ states were influenced by the anions, while the fast evolution from initially excited $^4T_2$ or ^{4}LMCT states to the doublet manifold (ISC, VC, IC) remained unaffected [100].

The *Molecular Ruby* **Cr5**$^{3+}$ features acidic methylene bridges in the ligand due to the high positive charge. Deprotonation of **Cr5**$^{3+}$ is reversible and forms a non-emissive complex. Therefore, addition of an acid is required to prevent deprotonation and to harvest the full luminescence potential of **Cr5**$^{3+}$. The acidic protons also lead to a stronger interaction with solvent molecules and counter ions via hydrogen bonding. As a result, in deaerated $D_2O/DClO_4$ quantum yields of 13.4, 15.7 and 20.0% were obtained for the [BF$_4$]$^-$, [ClO$_4$]$^-$ and [PF$_6$]$^-$ salts of **Cr5**$^{3+}$, respectively [73].

4 Tuning emission energy in *Molecular Rubies*

In charge-transfer emitters (LMCT, MLCT, LL'CT), it is straightforward to tune excited state energies for example by introducing electron-donating or -withdrawing substituents on the ligand [101–103]. Methods for tuning the energy of metal-centered spin-flip states are not so obvious [27, 73, 88]. Their energies depend on the nephelauxetic effect, i.e., the covalency of the metal–ligand bond and the Racah parameters B and C [50, 57]. The archetypical *Molecular Ruby* **Cr4**$^{3+}$ and many of its congeners emit in the NIR-I spectral region between 720 and 780 nm [25, 27, 28, 64, 78, 85]. By increasing the metal–ligand covalency with a monoanionic carbazolato ligand in $[Cr^{III}(dpc)_2]^+$ **Cr13**$^+$ ($dpc^- = $ 3,6-di-tert-butyl-1,8-di(pyridine-2-yl)-carbazolato; Scheme 1, Table 1), the emission band shifted to the NIR-II peaking at 1067 nm in frozen solution at 77 K [87]. The high covalency of the bond between Cr^{III} and the anionic ligand ($B = 470–550\ cm^{-1}$) decreased the repulsion of the d electrons and led to an unprecedentedly low energy of the spin-flip emission. However, an admixed ^{2}LMCT state in **Cr13**$^+$ increased the excited state distortion which facilitated non-radiative relaxation to the ground state leading to a low quantum yield of $\Phi < 0.00089\%$ and a relatively short lifetime of $\tau_1 = 1.4\ \mu s$ (88%) and $\tau_2 = 6.3\ \mu s$ (12%) at 77 K. In addition, it is plausible to assume that multi-phonon relaxation of the excited state (see above) plays a significant role because the NIR-II emission band might have a large spectral overlap with the absorption bands of the ligands' aromatic C–H overtones [87]. Similarly a low-energy phosphorescence at 910 nm was found for *fac*-$Cr^{III}(ppy)_3$ **Cr14** (ppy = anion of 2-phenylpyridine; Scheme 1, Table 1), an isostructural analog of the famous CT emitter $Ir^{III}(ppy)_3$, with a lifetime of 9.5 µs in 2-MeTHF (2-MeTHF = 2-methyltetrahydrofuran) at room temperature. At 77 K, the maximum shifted to 890 nm with shoulders at 910 and 1020 nm and a lifetime of 48 µs. The low quantum yield of 0.03% at room temperature in dichloromethane solution was rationalized with multiphonon quenching via C–H oscillators of the ligands, trigonal distortion in the excited state reminiscent of $[Cr^{III}(bpy)_3]^{3+}$ **Cr8**$^{3+}$ and self-quenching enabled by intermolecular π–π and CH–π interactions of this neutral complex **Cr14** [88].

In Cr^{III} complexes with amine ligands like **Cr1**$^{3+}$, **Cr10**$^{3+}$ or $[Cr^{III}(NH_3)_6]^{3+}$ **Cr15**$^{3+}$, a weak red emission between 657 and 690 nm was observed, but lifetimes and quantum yields were poor (Scheme 1, Table 1) [63, 84, 104]. Recently, the emission maximum of a highly emissive *Molecular Ruby* was successfully blue-shifted to 709 nm by employing a methylene-bridged tripyridine ligand in **Cr5**$^{3+}$ [73]. Compared to **Cr4**$^{3+}$, this marks an increase of 1200 cm^{-1} in doublet state energy. This trend was correctly predicted by complete active space self-consistent field calculations with N-electron valence perturbation correction (CASSCF(7,12)-NEVPT2) [73].

A theoretical upper limit of the emission energy can be derived from ligand field theory using the Racah parameter B of the central metal ion. Assuming $C/B = 4.0$, a ^{2}E energy of 19.5 B is predicted for an octahedral d^3 complex [58]. With $B = 918\ cm^{-1}$ for the free Cr^{3+} ion [50], this corresponds to 17,900 cm^{-1} (559 nm). The doublet state energies are also determined by the ratio C/B. This is nicely demonstrated by ruby ($Al_2O_3:Cr^{3+}$) which features a highly ionic metal ligand bond with $B = 822\ cm^{-1}$ but due to the low ratio $C/B = 3.2$ merely shows red emission at 694 nm (14,400 cm^{-1}) [105].

An alternative strategy to ligand design for the tuning of the emission energy is changing the central metal ion. A lower charge and/or extended d-orbitals as in 4d/5d transition metals result in a lower interelectronic repulsion. Consequently, highly charged central ions like Mn^{IV} ($B = 1064\ cm^{-1}$) [50] should in principle lead to high spin-flip energies. However, in the end the covalence of the metal–ligand bond is the decisive factor, which needs to be considered for each complex individually. A more detailed discussion can be found in Sect. 6.

5 Applications

The phosphorescence of Cr^{III} emitters is quenched by triplet dioxygen $^3O_2$ via doublet-singlet Dexter-type energy transfer forming $^1O_2$ with 61% quantum yield in the case of **Cr4**$^{3+}$. This excited state reactivity allows utilizing **Cr4**$^{3+}$ as an optical oxygen sensor and as photosensitizer for the α-cyanation of aliphatic amines via $^1O_2$/trimethylsilylcyanide [25, 74].

The complex **Cr12**$^{3+}$ (Scheme 1, Table 1) was successfully employed as a photoredox catalyst in radical cationic [4 + 2] cycloaddition reactions [106]. Photoexcited **Cr12**$^{3+}$ is reductively quenched by the substrate (e.g., *trans*-anethol). The resulting radical cation reacts with a diene like isoprene. Interestingly, the catalysis requires the presence of O_2 likely functioning as an electron shuttle. Oxygen can oxidize **Cr12**$^{2+}$ to regenerate the photocatalyst **Cr12**$^{3+}$ and to form superoxide. Finally, superoxide reduces the cationic intermediate after reaction of the oxidized alkene and the diene yielding the [4 + 2] cycloaddition product [86, 107]. This catalytic scheme strongly benefits from the very long excited state lifetime of 13 µs of **Cr12**$^{3+}$ in CH_3NO_2 even under aerobic conditions [86].

Cr4^{3+} shows dual phosphorescence from its doublet states at 738 and 775 nm at room temperature because these two states are in thermal equilibrium with an energy difference of 650–700 cm^{-1} [108]. Thus, the complex was employed as a self-referenced ratiometric optical temperature sensor [108, 109].

Hydrostatic pressures for example in diamond anvil cells are usually measured optically via the shift in emission energies of ruby's R_1/R_2 lines (approx. –0.77(3) and –0.84(3) cm^{-1} $kbar^{-1}$) [110, 111]. Interestingly, for **Cr4**$[BF_4]_3$ much larger shifts of –14.8 and –9.5 cm^{-1} $kbar^{-1}$ were found for the low- and high-energy emission, respectively, in aqueous solution, in methanol and in the solid state. The large barochromic effect is explained by subtle changes in the coordination geometry of the complex induced by high pressures [72, 112].

The high doublet energy and long excited state lifetime of the spin-flip state of **Cr5**$^{3+}$ allowed for a Dexter-type doublet-triplet energy transfer to 9,10-diphenylanthracene followed by efficient green-to-blue triplet–triplet annihilation upconversion (2 × 532 nm → 432 nm) with a high quantum yield of 12.0% (maximum value is 50%) [113]. The long-lived excited states in Cr^{III} complexes can also be used to increase the excited state lifetime of lanthanide ions via $Cr^{III} \rightarrow Ln^{III}$ energy transfer as exemplified by binuclear $[Cr^{III}Ln^{III}(L^1)_3]^{6+}$ ($Ln^{III} = Nd^{III}$: **CrNd**, $Ln^{III} = Yb^{III}$: **CrYb**, Fig. 3a and 3b) and trinuclear $[Cr^{III}Ln'^{III}Cr^{III}(L^2)_3]^{9+}$ helicate complexes ($Ln'^{III} = Nd^{III}$: **CrNdCr**, $Ln'^{III} = Er^{III}$: **CrErCr**, $Ln'^{III} = Yb^{III}$: **CrYbCr**, Fig. 3a, c). Using the $^4A_2 \rightarrow {}^2E$ excitation of the Cr^{III} centers at 750 nm, lifetimes in the millisecond region were reached for the lanthanide emissions between 1000 and 1670 nm [114, 115]. For **CrNdCr** and **CrYbCr** quantum yields of 2.7(1) and 3.0(3) % were determined, respectively [115]. Furthermore, **CrErCr** (Fig. 3c) yielded green upconverted Er^{III} emission ($^4S_{3/2} \rightarrow {}^4I_{15/2}$) with NIR irradiation via a sequential energy transfer upconversion (ETU) process (2 × 750 nm → 543 nm) in the solid state at 10 K and in frozen CH_3CN solution at 30 K. The efficiency of the $Cr^{III} \rightarrow Er^{III}$ energy transfer amounts to 50% [116].

Alternatively, the *Molecular Ruby* **Cr4**$^{3+}$ operated as energy acceptor in a cooperative upconversion process from the $^2F_{7/2} \rightarrow {}^2F_{5/2}$ transition of Yb^{3+} in the [**Cr4**]$[Yb^{III}(dpa)_3]$ double salt yielding NIR-to-NIR upconverted photons (2 × 980 nm → 775 nm; dpa = 2,6-pyridine-dicarboxylate) [117].

A particularly promising application of spin-flip emission is circularly polarized luminescence (CPL) with potential applications like biosensing, telecommunication and security inks [118–121]. Unlike tpy, ligands like ddpd or dqp^{OMe} (dqp^{OMe} = 2,2´-(4-methoxypyridine-2,6-diyl)diquinoline) employed in *Molecular Rubies* form six-membered chelate rings with boat conformations. Two enantiomers (*P*,*P*) and (*M*,*M*) arise from the resulting double helix of the ligands around the central ion (Fig. 4). In several instances, a separation was possible using HPLC with chiral stationary phases.

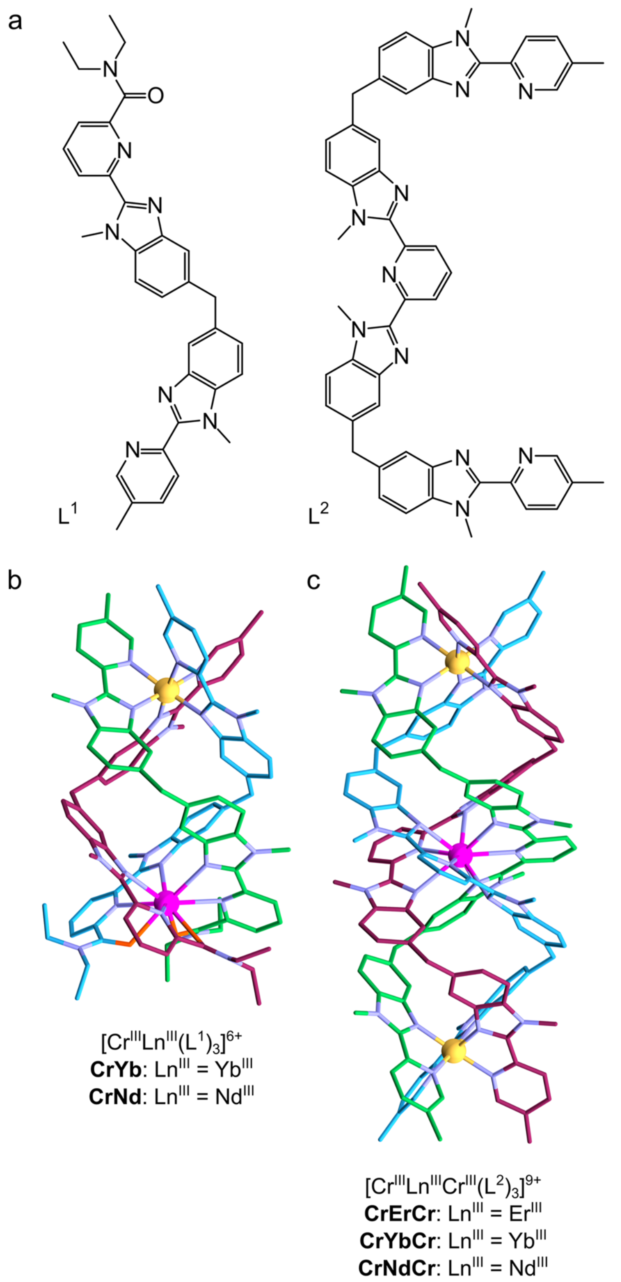

$[Cr^{III}Ln^{III}(L^1)_3]^{6+}$
CrYb: $Ln^{III} = Yb^{III}$
CrNd: $Ln^{III} = Nd^{III}$

$[Cr^{III}Ln^{III}Cr^{III}(L^2)_3]^{9+}$
CrErCr: $Ln^{III} = Er^{III}$
CrYbCr: $Ln^{III} = Yb^{III}$
CrNdCr: $Ln^{III} = Nd^{III}$

Fig. 3 Structures of **a** ligands L^1 and L^2, **b** binuclear Cr^{III}–Ln^{III} complexes and **c** trinuclear Cr^{III}–Ln^{III}–Cr^{III} complexes [114–116] with red, green and blue colors used for carbon atoms on different ligands; chromium colored in yellow; lanthanide in violet; nitrogen colored in gray; oxygen colored in orange; hydrogen atoms were omitted for clarity

Apart from rich electronic circular dichroism, the separated enantiomers also showed strong CPL [28, 29, 122–124]. The key figure for quantification is the dissymmetry factor g_{lum} representing the excess of left-handed polarized over right-handed polarized light intensity I_L and I_R (Eq. 5). The physical description of g_{lum} (Eq. 5) includes the electronic and magnetic transition dipole moments $|\mu_{ab}|$ and $|m_{ba}|$,

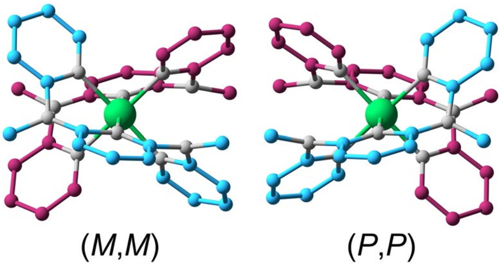

Fig. 4 Molecular structures of enantiomers of $[Cr^{III}(ddpd)_2]^{3+}$ **Cr4**$^{3+}$ with red and blue colors used for carbon atoms on different ddpd ligands to clarify each ligand's helicity; chromium colored in green; nitrogen colored in gray; hydrogen atoms were omitted for clarity [122]

respectively, as well as the angle τ_{ab} between the two vectors. Equation 5 shows that a high dissymmetry factor g_{lum} is expected for transitions a → b which are spin-forbidden (low $|\mu_{ab}|$) and magnetic dipole allowed (high $|m_{ba}|$) [125]. Both conditions are met by the $^2E \rightarrow {}^4A_2$ transition in *Molecular Rubies* yielding outstanding $|g_{lum}|$ values of 0.09 for **Cr4**$^{3+}$ and 0.20 for $[Cr^{III}(dqp^{OMe})_2]^{3+}$ **Cr16**$^{3+}$ (Scheme 1, Table 1) [29, 122]. Dissymmetry factors as high as this are rarely achieved with CT emitters and usually necessitate the use of lanthanide complexes exploiting metal-centered *ff*-transitions [123, 125, 126].

$$g_{lum} = \frac{I_L - I_R}{0.5\left(I_L + I_R\right)} = \frac{\Delta I}{I} \approx 4\frac{\left|m_{ba}\right|}{\left|\mu_{ab}\right|}\cos\tau_{ab}. \quad (5)$$

Intraconfigurational spin-flip transitions can potentially be exploited in optically addressable qubits. Complexes of Cr^{III}, Cr^{IV}, V^{III} and Ni^{II} like **Cr4**$^{3+}$, **Cr17–Cr22**, **V4**, **Ni1**$^{2+}$ and **Ni2**$^{2+}$ (Tables 1 and 2, Schemes 1, 2 and 5) were proposed as suitable candidates [127–132]. Their properties are discussed in more detail below.

6 Spin-flip emitters based on other transition metals and electronic configurations

This section highlights spin-flip emissive complexes of 3*d*, 4*d* and 5*d* metal ions with suitable *d* electron configurations.

Table 2 Optical properties of luminescent V^{III} and Cr^{IV} complexes with emission maximum λ_{max}, luminescence lifetime τ and quantum yield Φ measured in absence of oxygen

Number	Complex	Medium	λ_{max}/nm	τ/ns	Φ/%	References
V1^{3+}	$[V^{III}(urea)_6]^{3+}$	Solid (77 K)	992, 1010, 1011, 1187	–	–	[140]
V2^{3+}	$[V^{III}(ddpd)_2]^{3+}$	CD_3CN (298 K)	982, 1088, 1109	1351^a	1.8×10^{-4}	[62]
			374, 447, 660	2.2^b	2.1	[62]
V3	*mer*-$V^{III}Cl_3(ddpd)$	Solid (298 K)	1102, 1219, 1256	500	–	[144]
V4	$V^{III}\{(C_6F_5)_3tren\}(CN^tBu)$	2-MeTHF (77 K)	1240	9220^c	–	[128]
		Single crystal (298 K)	1250	3040	–	[128]
Cr17	$Cr^{IV}(CH_2CPh_3)_4$	In $Sn^{IV}(L)_4$ host crystal (4 K) ^{d}	≈920	–	–	[131]
Cr18	$Cr^{IV}(CH_2TMS)_4$ ^{e}	In isostructural Sn^{IV} Host crystal (4 K)	923	–	–	[131]
Cr19	$Cr^{IV}(cyclohexyl)_4$	In isostructural Sn^{IV} Host crystal (4 K)	897	–	–	[131]
Cr20	Cr^{IV}(*o*-tolyl)$_4$	In isostructural Sn^{IV} Host crystal (4 K)	1025	3300	–	[130, 131]
Cr21	Cr^{IV}(2,3-dimethylphenyl)$_4$	In isostructural Sn^{IV} Host crystal (4 K)	1009	6900	–	[130, 131]
Cr22	Cr^{IV}(2,4-dimethylphenyl)$_4$	In isostructural Sn^{IV} Host crystal (4 K)	1025	5700	–	[130, 131]

[a] Amplitude averaged lifetime based on biexponential decay with $\tau_1 = 790$ ns (0.93) and $\tau_2 = 8800$ ns (0.07)

[b] Amplitude averaged lifetime based on biexponential decay with $\tau_1 = 3.2$ ns (0.56) and $\tau_2 = 8.2$ ns (0.44)

[c] Determined at 90 K

[d] L = 2,4-dimethylphenyl

[e] CH_2TMS = (trimethylsilyl)methyl.

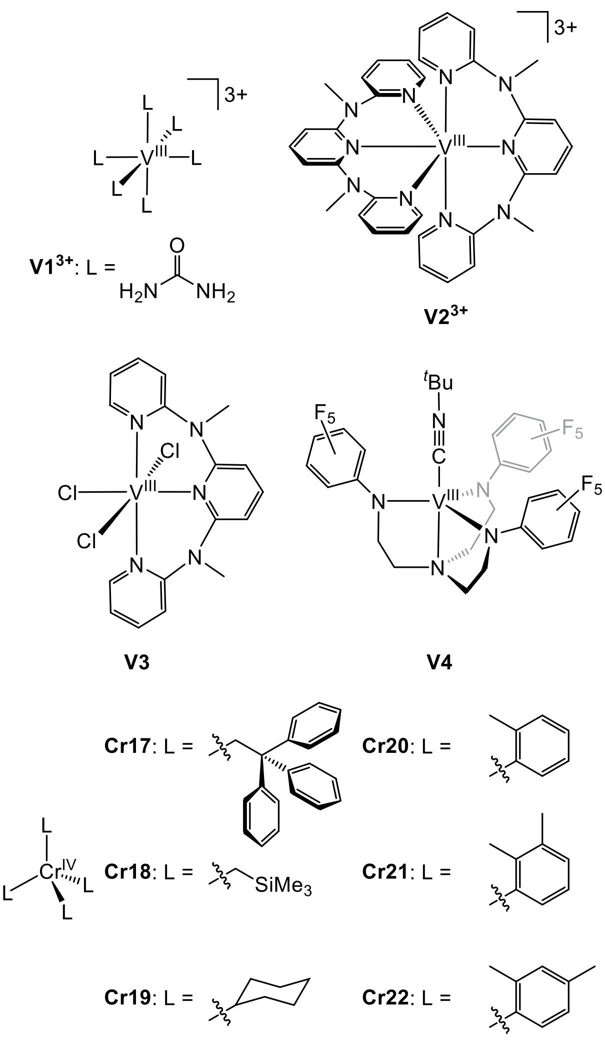

Scheme 2 Structures of luminescent V^{III} and Cr^{IV} complexes [62, 128, 130, 131, 142, 144]

6.1 d^2 – Ti^{II}, V^{III}, Cr^{IV}, Mo^{IV}, Tc^{V}, Re^{V}

The relevant excited states for spin-flip emission in the d^2 configuration in an octahedral field are the $^3T_1$ ground state, the interconfigurational $^3T_2$ and intraconfigurational $^1T_2$/^1E excited states (Fig. 1a).

Divalent group 4 metal ions are potential candidates for spin-flip emissive d^2 complexes [37, 38]. However, stable complexes of, e.g., Ti^{II} are quite rare and their investigation so far focused on electrochemical properties and reactivity [133–139]. Thus, no spin-flip luminescence with Ti^{II} complexes has been reported to date, while examples for luminescent solid-state materials containing Ti^{2+}, such as $MgCl_2$:Ti^{2+} and NaCl:Ti^{2+}, exist [37, 38].

A weak, structured emission was found for [V^{III}(urea)$_6$]$^{3+}$ **V1^{3+}** at 77 K in the solid state peaking at 992, 1010, 1011 and 1187 nm (Table 2) [140–142]. Trigonal Jahn–Teller distortion splits the $^3T_1$ ground state by 1400 cm^{-1} to $^3A_1$ and ^3E states. This ground-state splitting of octahedral d^2 metal complexes is a key difference to d^3 spin-flip emitters with their orbitally non-degenerate $^4A_2$ ground state (Fig. 1a,b). In V^{III} complexes, the total luminescence intensity is distributed to a large number of possible spin-flip transitions $^1T_2$/^1E → $^3T_1$ with differing energies [143].

[V^{III}(ddpd)$_2$]$^{3+}$ **V2^{3+}** is the first V^{III} complex showing NIR luminescence at room temperature in solution (Scheme 2, Table 2). This was achieved by using the strong σ-donor ddpd that has been previously employed in the first *Molecular Ruby* [25, 62]. The ligand field splitting is so large that the complex is located well above the first crossing point ($^1T_2$, ^1E)/$^3T_2$, placing the spin-flip states below the interconfigurational $^3T_2$ states in the TS diagram (Fig. 1a). When excited at 306 nm, **V2^{3+}** shows a weak NIR-II phosphorescence peaking at 982, 1088 and 1109 nm in solution at 298 K. The bands were assigned to the spin-flip transitions from $^1T_2$/^1E to the split $^3T_1$ ground state. A quantum yield of 0.00018% was found for this NIR-II emission in CD_3CN at room temperature. Low energy excitation at 620 nm is less efficient in populating the metal-centered $^1T_2$/^1E states. In butyronitrile at 77 K, the luminescence decayed biexponentially with lifetimes of $\tau_1 = 790$ ns (93%) and $\tau_2 = 8800$ ns (7%). In addition to the NIR-spin-flip emission, blue fluorescence possibly originating from a ^{3}LMCT state was detected at 396 nm in CD_3CN at 298 K with a high quantum yield of 2.1%. This dual emissive behavior was rationalized with an inefficient ISC and fast spin-allowed IC and fluorescence. In contrast to **Cr4^{3+}**, non-radiative deactivation of the low-energy $^1T_2$/^1E spin-flip states via multiphonon relaxation (electronic-to-vibrational energy transfer to vibrational overtones of C–H oscillators) unexpectedly does not play a significant role as evidenced by the very similar lifetimes and quantum yields of the non-deuterated and perdeuterated vanadium(III) complexes [62, 79]. The low quantum yield can then be attributed to a poor ISC efficiency and efficient non-radiative decay pathways beyond multiphonon relaxation. Possibly the inefficient ISC may be caused by the low density of acceptor states in the singlet manifold as Δ_O in **V2^{3+}** lies below the second triplet-singlet crossing point $^1A_1$/$^3T_2$ in the TS diagram (Fig. 1a) [62].

NIR-II spin-flip emission was also detected for the heteroleptic complex *mer*-V^{III}Cl$_3$(ddpd) **V3** (Scheme 2, Table 2) in the solid state at room temperature with bands at 1102, 1219 and 1256 nm and a phosphorescence lifetime of 0.5 µs [144]. Ligand deuteration significantly increased the phosphorescence lifetime to 3.4 µs. Transient absorption spectroscopy showed that the long-lived singlet states are populated after $\tau = 1.4$ ps, which is an upper limit for the time constant of the ISC. Trajectory surface hopping simulations within a linear vibronic coupling model arrived at a similar value of 1.7 ± 0.3 ps [145]. Interestingly, under hydrostatic pressure **V3** showed a hypsochromic shift by + 10 cm^{-1} kbar^{-1}

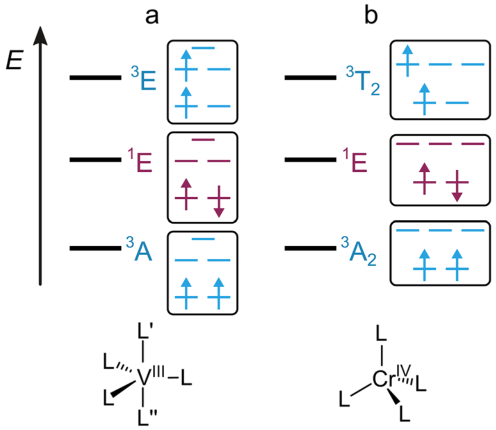

Fig. 5 Schematic energy-level ordering and exemplary microstates in **a** trigonal–bipyramidal V^{III} complex **V4** and **b** tetrahedral Cr^{IV} complexes **Cr17**–**Cr22** (Scheme 2, Table 2) [128, 130, 147]

in contrast to the bathochromic shifts found for $\mathbf{Cr4^{3+}}$. This positive shift was rationalized by the combined effect of changes in singlet energy and ground state splitting under pressure [144].

Spin-flip emission occurs also in five-coordinate $V^{III}\{(C_6F_5)_3tren\}(CN^tBu)$ **V4** ($\{(C_6F_5)_3tren\}^{3-}$ = 2,2',2''-tris[(pentafluorphenyl)amido]trimethylamine; Scheme 2, Table 2) which was proposed as an optically addressable molecular quantum bit candidate [128]. In this coordination geometry, a ^3A ground state and ^3E and ^1E MC excited states arise (Fig. 5a). Excitation at 640 nm assigned as a spin-allowed $^3A \rightarrow {}^3E$ transition yielded a $^1E \rightarrow {}^3A$ emission around 1240 nm in 2-MeTHF at 77 K and in single crystals. No emission was detected at room temperature in fluid solution. Long lifetimes of 11.1 and 3.0 µs were measured of single crystals of **V4** at 4 K and at room temperature, respectively, substantiating the assignment of the emission as phosphorescence. ISC was found to occur within < 4.2 ps followed by VR with a time constant of 26 ps [128]. The rather slow ISC compared to **V3** [144] or $Cr^{III}(acac)_3$ **Cr3** (Scheme 1) [68, 146] was attributed to restrictions of vibrational modes along the ISC reaction coordinate imposed by the rigid substituted tren ligand [128].

The TS diagram of tetrahedral d^2 complexes is analogous to the octahedral d^8 case (Figs. 1d and 5b). Hence spin-flip emission from a $^1E \rightarrow {}^3A_2$ transition could be achieved with a high ligand field splitting in tetrahedral d^2 complexes [147]. In fact, tetrahedral Cr^{IV} complexes with anionic alkyl or aryl ligands **Cr17**–**Cr22** emit between 897 and 1025 nm at 4 K and were proposed as optically addressable qubit candidates (Scheme 2, Table 2) [130, 131]. For the investigation, the complexes **Cr18**–**Cr22** were diluted in isostructural Sn^{IV} host lattices while a Sn^{IV}(2,4-dimethylphenyl)$_4$ lattice was used for $Cr^{IV}(CH_2CPh_3)_4$ **Cr17** ($CH_2CPh_3^-$ = 2,2,2-triphenyleth-1-yl). A resulting incompatibility with this host lattice in **Cr17** served to explain its broad emission compared to the extremely narrow bandwidths obtained for **Cr18**–**Cr22**. Because of the stronger nephelauxetic effect in the aryl complexes **Cr20**–**Cr22**, their emission is of lower energy than in the alkyl derivatives **Cr17**–**Cr19** [131]. The phosphorescence lifetimes of **Cr20**–**Cr22** in the host lattices at 4 K were determined as 3.3, 5.7 and 6.9 µs, respectively [130].

Long-lived phosphorescence from oxido and nitrido complexes featuring M=O, O=M' = O or M'≡N (M = Mo^{IV}; M' = Tc^V, Re^V, Os^{VI}) moieties is well known [148–154]. Although all of these complexes feature a d^2 electronic configuration, their emission does not arise from an *intra*-configurational spin-flip state but rather from an *inter*configurational MC states. The complexes' D_{4h} symmetry and strong π-bonds to the nitrido or oxido ligands give rise to a $^1A_1$ ground state with $(d_{xy})^2$ configuration and an emissive ^3E state with $(d_{xy})^1(d_{yz}, d_{xz})^1$ configuration [148–154], which is distinctly different from the $^3T_1$ ground state and $^1T_2/^1E$ spin-flip states expected for octahedral d^2 complexes (Fig. 1a) [50].

6.2 d^3 – Mo^{III}, WIII, VII, Mn^{IV} and Re^{IV}

Luminescent molecular Cr^{III} complexes have been known for a long time with many reviews covering this substance class [56, 63, 143, 155, 156, 158]. In contrast to Cr^{III}, luminescent complexes of Mo^{III} and W^{III} were hardly investigated. To our knowledge, ten emissive molecular Mo^{III} complexes and only one emissive W^{III} complex were reported in three publications [159–161]. This is probably due to the fact that Mo^{III} and W^{III} complexes are less stable than Cr^{III} complexes despite their $(t_{2g})^3$ electronic configuration [162]. It was suggested that the higher ionic radii facilitate decomposition via seven-coordinate intermediates or that decomposition may be catalyzed by byproducts with different oxidation states [162]. In general, intermediate oxidation states like + III are more difficult to stabilize in 5*d* and 6*d* transition metal complexes resulting in complexes sensitive to oxidation [163, 164].

Mo^{III} and W^{III} ions provide a very high intrinsic ligand field splitting due to better overlap of the large 4*d* and 5*d* orbitals with orbitals of the coordinating ligands. In addition, the heavier elements enable strong SOC, which is expected to enhance ISC rates [161, 165–167]. Absorption spectroscopy revealed that even with weak π-donating ligands like chloride in $[Mo^{III}Cl_6]^{3-}$ $\mathbf{Mo1^{3-}}$ the $^4T_2$ state is located well above the $^2E/^2T_1/^2T_2$ states and thus Δ_O is past the first and second crossing points in the TS diagram (Fig. 1b) [160]. The emission bands of the known Mo^{III} complexes $\mathbf{Mo1^{3-}}$, $[Mo^{III}(NCS)_6]^{3-}$ $\mathbf{Mo2^{3-}}$, *mer*-$Mo^{III}Cl_3(L)_3$ **Mo3**–**Mo5** (L = py, urea, tu; py = pyridine, tu = thiourea), *mer*-$Mo^{III}Br_3(urea)_3$ **Mo6**, *fac*-$Mo^{III}(Me_3[9]aneN_3)X_3$

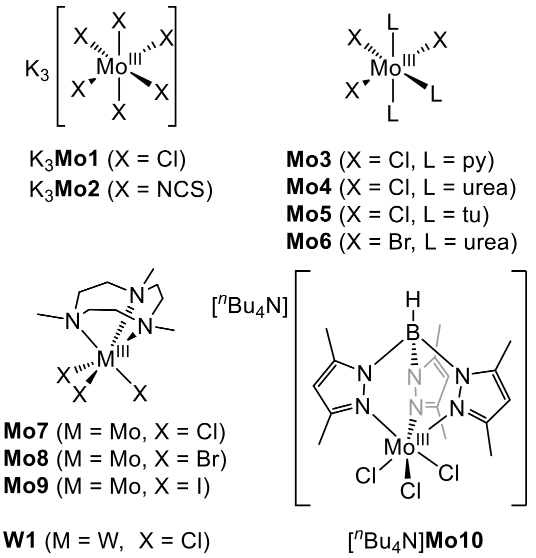

K_3**Mo1** (X = Cl)
K_3**Mo2** (X = NCS)

Mo3 (X = Cl, L = py)
Mo4 (X = Cl, L = urea)
Mo5 (X = Cl, L = tu)
Mo6 (X = Br, L = urea)

Mo7 (M = Mo, X = Cl)
Mo8 (M = Mo, X = Br)
Mo9 (M = Mo, X = I)

W1 (M = W, X = Cl)

[^{n}Bu$_4$N]**Mo10**

Scheme 3 Structures of luminescent Mo^{III} and W^{III} complexes [159–161]

Mo7–**Mo9** (Me$_3$[9]aneN$_3$ = 1,4,7-trimethyl-1,4,7-triazacyclononane; X = Cl, Br, I) and *fac*-[Mo^{III}{HB(Me$_2$Pz)$_3$}Cl$_3$]$^-$ **Mo10**$^-$ ({HB(Me$_2$Pz)$_3$}$^-$ = tris(3,5-dimethyl-1*H*-pyrazol-1-yl)hydroborate) appear between 1090 and 1400 nm with emission lifetimes of several hundred nanoseconds and poor quantum yields of 0.0061–0.012% (Scheme 3, Table 3) [160, 161]. Multiphonon relaxation via C–H oscillators of the ligands or solvent molecules might play an important role in the deactivation of the excited states. Another reason for the poor quantum yields measured for **Mo7**–**Mo9** might be that despite the high SOC in Mo^{III} [165], ISC could be slow due to a low density of doublet states in the region of the initially excited $^4T_2$ state at the FC geometry. For W^{III}Cl$_3$(Me$_3$[9]aneN$_3$) **W1** (Scheme 3, Table 3) the emission peaked at 1400 nm, but the complex was too unstable for a more detailed investigation [161]. The trend of the energies going from Cr^{III} to Mo^{III} and W^{III} can be explained with respect to the weaker interelectronic repulsion in this series (Cr^{3+}: $B = 918$ cm^{-1}, Mo^{3+}: $B = 610$ cm^{-1}) [50, 161].

Investigations of novel Mo^{III} and W^{III} emitters may offer insights on the effects that very high ligand field splittings Δ_O have on the efficiency of the ISC processes and the radiative and non-radiative rates for the spin-flip state relaxation. Applying the lessons learned from the *Molecular Rubies* might help in the design and synthesis of stable Mo^{III} and W^{III} complexes with strong emission in the NIR-II spectral region.

Vanadium(II) complexes also feature a d^3 electronic configuration and are thus potential candidates for spin-flip emission similar to Cr^{III}. The Racah parameter $B(V^{2+}) = 766$ cm^{-1} of the free ion is lower compared to $B(Cr^{3+}) = 918$ cm^{-1} [50] indicating lower doublet energies for V^{II} complexes [89]. However, the lower oxidation state also leads to a lower intrinsic ligand field splitting Δ_O [171]. In addition, a relatively facile oxidation of V^{2+} to V^{3+} may generate low-energy MLCT states. In fact, early studies on tris(bidentate)vanadium(II) complexes using bpy, bpy derivatives and phen **V5**$^{2+}$–**V8**$^{2+}$ (Scheme 4) concluded that their lowest excited states have ^{4}MLCT character. These complexes featured excited state lifetimes in the low nanosecond region and no luminescence [172]. The excited state assignment was recently called into question and a mixed ^{2}MC/^{2}MLCT state was proposed instead based on

Table 3 Optical properties of luminescent d^3 Mo^{III}, W^{III}, Mn^{IV} and Re^{IV} complexes with emission maxima λ_{max}, luminescence lifetimes τ and quantum yields Φ at room temperature

Number	Complex	Medium	λ_{max}/nm	τ/ns	Φ/%	References
K_3**Mo1**	$K_3[Mo^{III}Cl_6]$	Conc. HCl$_{(aq)}$	1095	480	–	[160]
K_3**Mo2**	$K_3[Mo^{III}(NCS)_6]$	MeCN	1350	760	–	[160]
Mo3	$Mo^{III}Cl_3(py)_3$	Solid	1400	–	–	[161]
Mo4	$Mo^{III}Cl_3(urea)_3$	Solid	1095	–	–	[159]
Mo5	$Mo^{III}Cl_3(tu)_3$	Solid	1090	–	–	[159]
Mo6	$Mo^{III}Br_3(urea)_3$	Solid	1105	–	–	[159]
Mo7	$Mo^{III}(Me_3[9]aneN_3)Cl_3$	MeCN	1120	960	0.0061	[161]
Mo8	$Mo^{III}(Me_3[9]aneN_3)Br_3$	MeCN	1130	800	0.0096	[161]
Mo9	$Mo^{III}(Me_3[9]aneN_3)I_3$	MeCN	1160	450	0.012	[161]
[^{n}Bu$_4$N]**Mo10**	[^{n}Bu$_4$N][Mo^{III}{HB(Me$_2$Pz)$_3$}Cl$_3$]	MeCN	> 1250	–	–	[161]
W1	$W^{III}(Me_3[9]aneN_3)Cl_3$	Solid	1400	–	–	[161]
K_2**Mn1**	$K_2[Mn^{IV}Cl_6]$	[a]	820	–	–	[168, 169]
Mn2(OTf)$_2$	[Mn^{IV}{PhB(MeIm)$_3$}$_2$](OTf)$_2$	Solid	600–750	50	–	[42, 43]
			814	1500	–	[42, 43]
[^{n}Bu$_4$N]$_2$**Re1**	[^{n}Bu$_4$N]$_2$[Re^{IV}Cl$_6$]	MeCN	1340	40–140	< 0.02	[160, 170]
[^{n}Bu$_4$N]$_2$**Re2**	[^{n}Bu$_4$N]$_2$[Re^{IV}Br$_6$]	MeCN	1380	–	–	[170]

[a] The measurements were performed in solution, but the detailed conditions were not reported

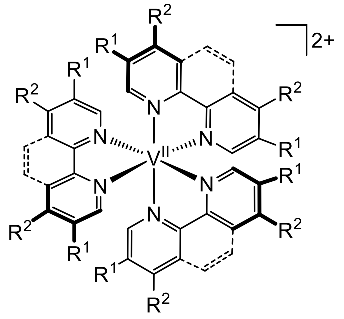

$V5^{2+}$: $R^1 = R^2 = H$, without dotted bonds
$V6^{2+}$: $R^1 = CH_3$, $R^2 = H$, without dotted bonds
$V7^{2+}$: $R^1 = H$, $R^2 = CH_3$, without dotted bonds
$V8^{2+}$: $R^1 = R^2 = H$, with dotted bonds

Scheme 4 Structures of V^{II} complexes discussed in the manuscript

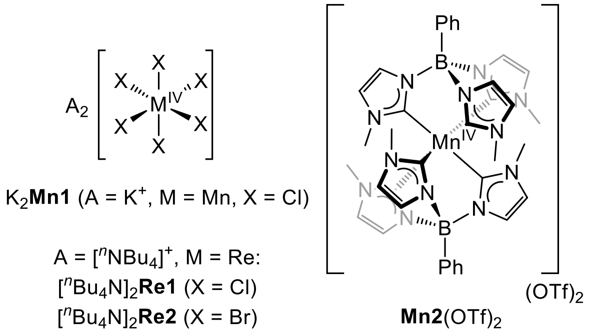

K_2**Mn1** (A = K^+, M = Mn, X = Cl)

A = $[^nNBu_4]^+$, M = Re:
$[^nBu_4N]_2$**Re1** (X = Cl)
$[^nBu_4N]_2$**Re2** (X = Br)

Mn2$(OTf)_2$

Scheme 5 Structures of luminescent Mn^{IV} and Re^{IV} complexes [42, 43, 160, 168–170]

electrochemical, quantum chemical and transient absorption studies [89]. The partial ^{2}MLCT character leads to geometric distortion facilitating non-radiative decay compared to Cr^{III} complexes with their nested doublet excited states [25]. Crystal structures of $[V^{II}(bpy)_3]^{2+}$ **$V5^{2+}$** and $[V^{II}(phen)_3]^{2+}$ **$V8^{2+}$** (Scheme 4) further revealed a significant trigonal distortion in the ground state. According to quantum chemical calculations, ISC pathways differ between **$V5^{2+}$/$V8^{2+}$** and their Cr^{III} homologues **$Cr8^{3+}$/$Cr9^{3+}$**. Both findings were rationalized with a stronger metal–ligand π-interactions in the V^{II} complexes [173].

Complexes of the heavier homologues Nb^{II} and Ta^{II} are rare and no spin-flip emission has been reported to date [137, 174–178].

For the d^3-ion Mn^{IV}, a very early report stated that $K_2[Mn^{IV}Cl_6]$ K_2**Mn1** emits at 820 nm in solution (Scheme 5, Table 3) [168, 169]. Apart from this, the only reported emissive complex is $[Mn^{IV}\{PhB(MeIm)_3\}_2](OTf)_2$ **Mn2**$(OTf)_2$ ($\{PhB(MeIm)_3\}^-$ = phenyltris(3-methylimidazol-2-yl)borate, Scheme 5, Table 3) [42, 43]. This hexacarbene complex shows a long-lived $^2E \rightarrow {}^4A_2$ spin-flip phosphorescence at 814 nm and a weak ^{4}LMCT fluorescence between 600 and 750 nm in the solid state at room temperature. When considering the higher Racah parameter of free Mn^{4+} (1064 cm^{-1}) compared to Cr^{3+} (918 cm^{-1}) [50], higher doublet state energies should be accessible in Mn^{IV} complexes. In **Mn2**$(OTf)_2$, however, the emission energy is lower than in most Cr^{III} complexes due to a high covalency of the bonds between the Mn^{IV} ion and the anionic tricarbene ligands (nephelauxetic effect) [42, 43, 57].

To the best of our knowledge, $[^nBu_4N]_2[Re^{IV}X_6]$ (X = Cl, Br) $[^nBu_4N]_2$**Re1** and $[^nBu_4N]_2$**Re2** (Scheme 5, Table 3) present the only emissive molecular Re^{IV} complexes in solution reported so far [160, 170]. Excitation at 360 and 414 nm in MeCN leads to NIR-II phosphorescence at 1340 and 1380 nm, respectively. For **$Re1^{2-}$**, lifetimes of 80 and 140 ns and an estimated upper limit of 0.02% for the quantum yield were reported [160, 170]. **$Re2^{2-}$** showed a phosphorescence lifetime of 40 ns and photosolvation upon LMCT excitation with UV light [179]. Analogous to the Mo^{III} and W^{III} cases, the extended 5*d* orbitals and low interelectronic repulsion in Re^{IV} lead to high-energy $^4T_2$ states and very low lying doublet states. The challenges accompanied with the heavier group 6 metal ions outlined above apply for Re^{IV} as well.

6.3 d^4 – Cr^{II}, Mo^{II}, WII, Mn^{III} and Re^{III}

The d^4 complexes are a special case among the electronic configurations discussed in this section. Depending on Δ_O, they can be high-spin or low-spin, resulting in dramatically different energy-level ordering (Fig. 1c). States of three different multiplicities (singlet, triplet, quintet) become relevant. Spin-flip emission is only conceivable in low-spin d^4 complexes. A very high Δ_O ($\gg 38\ B$ for $C/B = 4$) is required to establish the spin-flip states $^1T_2$ and ^1E as the lowest excited states below the high-spin state ^5E (Fig. 1c) [58]. The d^4 configuration is different from the others since deactivation of the potential spin-flip state via a $^1T_1 \rightarrow {}^5E$ transition would entail a change of the total spin of $\Delta S = 2$ instead of just 1. However, while efficient ISC processes with $\Delta S = 2$ are relatively rare, they cannot be excluded [180, 181]. Another challenge in this electronic configuration might be that the ^5E high-spin state always lies below the lowest triplet MC state ^3E. A relaxation cascade $^3E \rightarrow {}^1T_2/{}^1E$ after $^3T_1 \rightarrow {}^3E$ excitation is thus probably impeded by non-radiative deactivation of the ^3E state via the ^5E state similar to certain d^6-Fe^{II} complexes [19]. Therefore, in a potential d^4 spin-flip emitter, the $^1T_2$ and ^1E states need to be populated via other routes, e.g., CT states. Finally, similar to the d^2 electron configuration, the $^3T_1$ ground state of the low-spin d^4 electron configuration is orbitally degenerate giving rise to Jahn–Teller distortions (Fig. 1a,c). Overall, spin-flip emission from d^4 transition metal complexes has not been achieved yet for molecular systems. In principle complexes of group 6, ions in the oxidation state + II are potential candidates. However, there are only few examples of low-spin octahedral Cr^{II} complexes requiring exceptionally strong ligands like CN^{-} [182, 183]. The reduced *Molecular Ruby* [Cr^{II}(ddpd)$_2$]$^{2+}$ **Cr4^{2+}** shows spin-crossover at room temperature and dark excited states with microsecond lifetimes [184]. Further preparative and handling challenges for divalent group 6 metal ions include their sensitivity to oxidation, dimerization or cluster formation [185–190].

Other candidates for d^4 spin-flip emission are, e.g., Mn^{III}, Tc^{III} and Re^{III}. However, known emissive Mn^{III} complexes only show luminescence from ligand-centered transitions [191–194]. While octahedral Tc^{III} and Re^{III} complexes are quite common [195, 196], to the best of our knowledge no spin-flip emission has been reported so far.

Due to the very high Δ_O required for spin-flip emission in the d^4 case, complexes of 4*d* and 5*d* transition metal ions seem to be promising candidates.

6.4 *d*^{8} – Ni^{II}, Pd^{II} and Pt^{II}

In an octahedral ligand field, d^8 ions like Ni^{II} possess a $^3A_2$ ground state, a $^3T_2$ excited state and a ^1E spin-flip state (Fig. 1d). Compared to the other *d* electron configurations, the ^1E state in d^8 is unique because the spin-flip occurs in the e_g* orbitals with σ-instead of π-symmetry. Interestingly, the ^1E state consists of an unpaired and a spin-paired microstate (Fig. 1d). Population of the spin-paired microstate might lead to excited state Jahn–Teller distortion facilitating nonradiative decay to the ground state.

In principle, a strong ligand field could raise the $^3T_2$ state above the ^1E state and enable spin-flip phosphorescence. Octahedral Ni^{II} complexes with strong donor ligands like phen, tpm, bpy, tpy and ddpd (**Ni1^{2+}**–**Ni5^{2+}**; tpm = tris(pyrid-2-yl)methane; Scheme 6) show ligand field splittings of 17–18*B* which are close to the $^3T_2$/^1E crossing point in the TS diagram (Fig. 1d) [129, 197–201], while homo- and heteroleptic complexes with poly(pyrazolyl) methane ligands showed a lower Δ_O of 11–15*B* [202]. Absorption spectroscopy revealed that the $^3T_2$ and ^1E states are not sufficiently separated with ^1E transitions detected as shoulders on the $^3T_2$ bands. In this case, the spin-forbidden $^3A_2 \rightarrow {}^1E$ absorptions are enhanced by intensity borrowing from the nearby $^3T_2$ band [201]. The lowest energy adiabatic state is strongly anharmonic due to coupling with components of the $^3T_2$ state via SOC which reduces the spin-flip character [203]. In summary, a ligand field splitting $\Delta_O \gg 18B$ is necessary to bring spin-flip luminescence within reach [200]. However, as the classical example of [Ni^{II}(CN)$_4$]$^{2-}$ illustrates, a square-planar coordination geometry with a singlet ground state is favored with very strong ligands [204]. Thus, a balance between these two extremes is necessary for spin-flip emission.

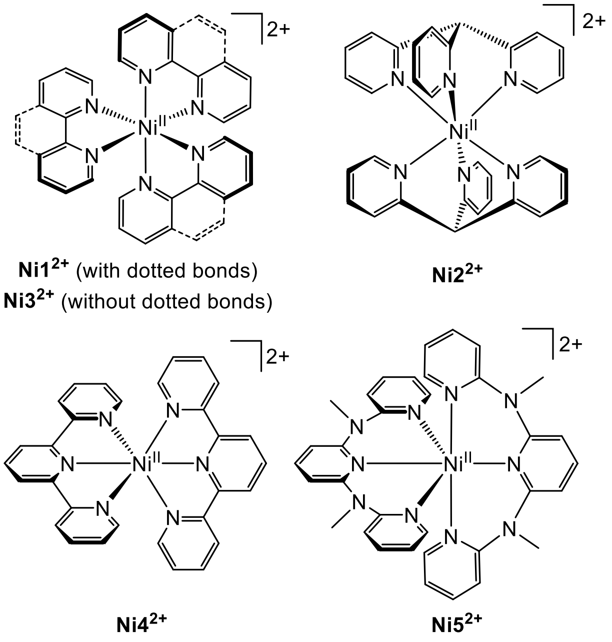

Scheme 6 Structures of Ni^{II} complexes discussed in the manuscript

It was reported that **Ni1^{2+}** and **Ni2^{2+}** are emissive in the solid state at 150 K [129]. However, these findings have been called into question since the reported emission bands for **Ni1^{2+}** and **Ni2^{2+}** are almost superimposable, which is unlikely considering their different symmetry [143].

The heavier homologues Pd^{II} and Pt^{II} prefer a square-planar coordination geometry due to their high intrinsic ligand field splitting [185]. Pseudooctahedral complexes of Pd^{II} and Pt^{II} are very rare and often require sophisticated ligands to avoid the formation of a square-planar geometry [205–210]. No spin-flip phosphorescence in these types of complexes was reported to date.

7 Conclusion

The numerous examples of spin-flip luminescent complexes in this review substantiate that metal-centered states can be more than just non-radiative relaxation pathways for charge-transfer states, but that spin-flip chromophores constitute a useful class of phosphorescent complexes complementary to charge-transfer chromophores. A deeper understanding of the requirements for efficient spin-flip emission has given rise to the emerging class of highly luminescent Cr^{III} complexes (*Molecular Rubies*) and the first luminescent V^{III} complexes. This marks substantial progress in the ongoing endeavor to establish photoactive complexes based on earth-abundant metals as sustainable alternatives to precious or rare earth metal complexes [11, 19, 158]. In this context, circularly polarized luminescence is a promising application of enantiopure chiral spin-flip emitters, which makes full use of their unique excited state properties [123].

This review also highlighted many open venues for more fundamental research. It is still a challenge to tune the relative energies of the relevant states to achieve, e.g., high-energy spin-flip emission. In addition, the role of the density of high-energy $^2T_2$ doublet states for efficient intersystem crossing in excited Cr^{III} complexes remains unclear to this date. 4*d* and 5*d* complexes of Mo^{III}, W^{III} or Re^{IV} offer ideal conditions to study d^3 spin-flip emission beyond the second quartet-doublet crossing point in the Tanabe-Sugano diagram. For some metal ions like Ni^{II}, reports on spin-flip emission are limited to doped solids [46], while convincing evidence in molecular systems is lacking. Here, it remains a challenge to establish a sufficiently high ligand field splitting that separates the initially excited interconfigurational states and the intraconfigurational spin-flip states without resulting in a square-planar coordination geometry.

Supplementary Information The online version contains supplementary material available at https://doi.org/10.1007/s43630-022-00186-3.

Acknowledgements The authors would like to thank Prof. Dr. Christian Reber, Dr. Christoph Förster and Nathan Roy East for constructive criticism of the manuscript. Parts of this research were conducted using the supercomputer ELWETRITSCH and advisory services offered by the Technical University of Kaiserslautern (https://elwe.rhrk.uni-kl.de/), which is a member of the AHRP.

Author contributions WRK conceptualized the article, performed the literature search and wrote the article. JM provided support in writing of the article. KH provided the idea and general concept for the article and critically revised the work. All authors read and approved the final manuscript.

Funding Open Access funding enabled and organized by Projekt DEAL. Financial support from the Deutsche Forschungsgemeinschaft [DFG, Priority Program SPP 2102 "Light-controlled reactivity of metal complexes" (HE 2778/13–1)] is gratefully acknowledged. W. R. K. is grateful to the Chemical Industry Funds for a Kekulé Fellowship.

Availability of data and material Supporting Information for quantum chemical calculations.

Code availability Not applicable.

Declarations

Conflicts of interest The authors declare no conflict of interest.

Ethics approval Not applicable.

Consent to participate Not applicable.

Consent for publication Not applicable.

Open Access This article is licensed under a Creative Commons Attribution 4.0 International License, which permits use, sharing, adaptation, distribution and reproduction in any medium or format, as long as you give appropriate credit to the original author(s) and the source, provide a link to the Creative Commons licence, and indicate if changes were made. The images or other third party material in this article are included in the article's Creative Commons licence, unless indicated otherwise in a credit line to the material. If material is not included in the article's Creative Commons licence and your intended use is not permitted by statutory regulation or exceeds the permitted use, you will need to obtain permission directly from the copyright holder. To view a copy of this licence, visit http://creativecommons.org/licenses/by/4.0/.

References

1. Bizzarri, C., Spuling, E., Knoll, D. M., Volz, D., & Bräse, S. (2018). Sustainable metal complexes for organic light-emitting diodes (OLEDs). *Coordination Chemistry Reviews, 373*, 49–82. https://doi.org/10.1016/j.ccr.2017.09.011
2. Li, X., Xie, Y., & Li, Z. (2021). Diversity of luminescent metal complexes in OLEDs: Beyond traditional precious metals. *Chemistry - An Asian Journal, 16*(19), 2817–2829. https://doi.org/10.1002/asia.202100784
3. Twilton, J., Le, C., Zhang, P., Shaw, M. H., Evans, R. W., & MacMillan, D. W. C. (2017). The merger of transition metal and photocatalysis. *Nature Reviews Chemistry*. https://doi.org/10.1038/s41570-017-0052
4. Imran, M., Ramzan, M., Qureshi, A. K., Khan, M. A., & Tariq, M. (2018). Emerging applications of porphyrins and metalloporphyrins in biomedicine and diagnostic magnetic resonance imaging. *Biosensors, 8*(4), 95. https://doi.org/10.3390/bios8040095
5. Chou, P.-T., & Chi, Y. (2006). Osmium- and ruthenium-based phosphorescent materials: Design, photophysics, and utilization in OLED fabrication. *European Journal of Inorganic Chemistry, 2006*(17), 3319–3332. https://doi.org/10.1002/ejic.200600364
6. Liu, Z., Bian, Z., & Huang, C. (2010). Luminescent iridium complexes and their applications. In H. Bozec & V. Guerchais (Eds.), *Molecular organometallic materials for optics* (pp. 113–142). Springer. https://doi.org/10.1007/978-3-642-01866-4_4
7. Mauro, M., Aliprandi, A., Septiadi, D., Kehr, N. S., & de Cola, L. (2014). When self-assembly meets biology: Luminescent platinum complexes for imaging applications. *Chemical Society Reviews, 43*(12), 4144–4166. https://doi.org/10.1039/c3cs60453e
8. Parker, D., Fradgley, J. D., & Wong, K.-L. (2021). The design of responsive luminescent lanthanide probes and sensors. *Chemical Society Reviews, 50*(14), 8193–8213. https://doi.org/10.1039/d1cs00310k
9. Shum, J., Leung, P.K.-K., & Lo, K.K.-W. (2019). Luminescent ruthenium(II) polypyridine complexes for a wide variety of biomolecular and cellular applications. *Inorganic Chemistry, 58*(4), 2231–2247. https://doi.org/10.1021/acs.inorgchem.8b02979
10. Wenger, O. S. (2019). Is iron the new ruthenium? *Chemistry--A European Journal, 25*(24), 6043–6052. https://doi.org/10.1002/chem.201806148
11. Förster, C., & Heinze, K. (2020). Photophysics and photochemistry with Earth-abundant metals—fundamentals and concepts. *Chemical Society Reviews, 49*(4), 1057–1070. https://doi.org/10.1039/c9cs00573k
12. Braun, J. D., Lozada, I. B., Kolodziej, C., Burda, C., Newman, K. M. E., van Lierop, J., Davis, R. L., & Herbert, D. E. (2019). Iron(II) coordination complexes with panchromatic absorption and nanosecond charge-transfer excited state lifetimes. *Nature Chemistry, 11*(12), 1144–1150. https://doi.org/10.1038/s41557-019-0357-z

13. Carey, M. C., Adelman, S. L., & McCusker, J. K. (2019). Insights into the excited state dynamics of Fe(II) polypyridyl complexes from variable-temperature ultrafast spectroscopy. *Chemical Science, 10*(1), 134–144. https://doi.org/10.1039/c8sc04025g
14. Fredin, L. A., Pápai, M., Rozsályi, E., Vankó, G., Wärnmark, K., Sundström, V., & Persson, P. (2014). Exceptional excited-state lifetime of an iron(II)-N-heterocyclic carbene complex explained. *Journal of Physical Chemistry Letters, 5*(12), 2066–2071. https://doi.org/10.1021/jz500829w
15. Dierks, P., Kruse, A., Bokareva, O. S., Al-Marri, M. J., Kalmbach, J., Baltrun, M., Neuba, A., Schoch, R., Hohloch, S., Heinze, K., Seitz, M., Kühn, O., Lochbrunner, S., & Bauer, M. (2021). Distinct photodynamics of κ-N and κ-C pseudoisomeric iron(II) complexes. *Chemical Communications, 57*(54), 6640–6643. https://doi.org/10.1039/d1cc01716k
16. Dierks, P., Päpcke, A., Bokareva, O. S., Altenburger, B., Reuter, T., Heinze, K., Kühn, O., Lochbrunner, S., & Bauer, M. (2020). Ground- and excited-state properties of iron(II) complexes linked to organic chromophores. *Inorganic Chemistry, 59*(20), 14746–14761. https://doi.org/10.1021/acs.inorgchem.0c02039
17. Reuter, T., Kruse, A., Schoch, R., Lochbrunner, S., Bauer, M., & Heinze, K. (2021). Higher MLCT lifetime of carbene iron(II) complexes by chelate ring expansion. *Chemical Communications, 57*(61), 7541–7544. https://doi.org/10.1039/d1cc02173g
18. Woodhouse, M. D., & McCusker, J. K. (2020). Mechanistic origin of photoredox catalysis involving iron(II) polypyridyl chromophores. *Journal of the American Chemical Society, 142*(38), 16229–16233. https://doi.org/10.1021/jacs.0c08389
19. Dierks, P., Vukadinovic, Y., & Bauer, M. (2022). Photoactive iron complexes: more sustainable, but still a challenge. *Inorganic Chemistry Frontiers*. https://doi.org/10.1039/D1QI01112J
20. Chábera, P., Kjær, K. S., Prakash, O., Honarfar, A., Liu, Y., Fredin, L. A., Harlang, T. C. B., Lidin, S., Uhlig, J., Sundström, V., Lomoth, R., Persson, P., & Wärnmark, K. (2018). FeII hexa N-heterocyclic carbene complex with a 528 ps metal-to-ligand charge-transfer excited-state lifetime. *Journal of Physical Chemistry Letters, 9*(3), 459–463. https://doi.org/10.1021/acs.jpclett.7b02962
21. Larsen, C. B., Braun, J. D., Lozada, I. B., Kunnus, K., Biasin, E., Kolodziej, C., Burda, C., Cordones, A. A., Gaffney, K. J., & Herbert, D. E. (2021). Reduction of electron repulsion in highly covalent Fe-amido complexes counteracts the impact of a weak ligand field on excited-state ordering. *Journal of the Chemical Society*. https://doi.org/10.1021/jacs.1c06429
22. Leis, W., Argüello Cordero, M. A., Lochbrunner, S., Schubert, H., & Berkefeld, A. (2022). A photoreactive iron(II) complex luminophore. *Journal of the Chemical Society*. https://doi.org/10.1021/jacs.1c13083
23. Viaene, L., & D'Olieslager, J. (1987). Luminescence from and absorption by the $^3T_{1g}$ level of the hexacyanocobaltate(III) ion. *Inorganic Chemistry, 26*(6), 960–962. https://doi.org/10.1021/ic00253a039
24. Kaufhold, S., Rosemann, N. W., Chábera, P., Lindh, L., Bolaño Losada, I., Uhlig, J., Pascher, T., Strand, D., Wärnmark, K., Yartsev, A., & Persson, P. (2021). Microsecond photoluminescence and photoreactivity of a metal-centered excited state in a hexacarbene-co(III) complex. *Journal of the American Chemical Society, 143*(3), 1307–1312. https://doi.org/10.1021/jacs.0c12151
25. Otto, S., Grabolle, M., Förster, C., Kreitner, C., Resch-Genger, U., & Heinze, K. (2015). $[Cr(ddpd)_2]^{3+}$: A molecular, water-soluble, highly NIR-emissive ruby analogue. *Angewandte Chemie International Edition, 54*(39), 11572–11576. https://doi.org/10.1002/anie.201504894
26. Förster, C., Dorn, M., Reuter, T., Otto, S., Davarci, G., Reich, T., Carrella, L., Rentschler, E., & Heinze, K. (2018). Ddpd as expanded terpyridine dramatic effects of symmetry and electronic properties in first row transition metal complexes. *Inorganics, 6*(3), 86. https://doi.org/10.3390/inorganics6030086
27. Doistau, B., Collet, G., Bolomey, E. A., Sadat-Noorbakhsh, V., Besnard, C., & Piguet, C. (2018). Heteroleptic ter-bidentate Cr(III) complexes as tunable optical sensitizers. *Inorganic Chemistry, 57*(22), 14362–14373. https://doi.org/10.1021/acs.inorgchem.8b02530
28. Jiménez, J.-R., Doistau, B., Cruz, C. M., Besnard, C., Cuerva, J. M., Campaña, A. G., & Piguet, C. (2019). Chiral molecular ruby $Cr(dqp)_2^{3+}$ with long-lived circularly polarized luminescence. *Journal of the American Chemical Society, 141*(33), 13244–13252. https://doi.org/10.1021/jacs.9b06524
29. Jiménez, J.-R., Poncet, M., Míguez-Lago, S., Grass, S., Lacour, J., Besnard, C., Cuerva, J. M., Campaña, A. G., & Piguet, C. (2021). Bright long-lived circularly polarized luminescence in chiral chromium(III) complexes. *Angewandte Chemie International Edition, 60*(18), 10095–10102. https://doi.org/10.1002/anie.202101158
30. Flint, C. (1971). A vibronic analysis of the transition in solid Cs_2MnF_6. *Journal of Molecular Spectroscopy, 37*(3), 414–422. https://doi.org/10.1016/0022-2852(71)90173-1
31. Chodos, S. L., Black, A. M., & Flint, C. D. (1976). Vibronic spectra and lattice dynamics of Cs_2MnF_6 and $A^1{}_2M^{IV}F_6$:$MnF6_2^-$. *The Journal of Chemical Physics, 65*(11), 4816–4824. https://doi.org/10.1063/1.432952
32. Flint, C. D., & Lang, P. F. (1987). Substitution reactions and luminescence spectra of the mixed complexes [ReClxBr 6–x]2–. *Journal of the Chemical Society, Dalton Transactions, 8*, 1929–1932. https://doi.org/10.1039/DT9870001929
33. Flint, C. D., & Lang, P. F. (1986). Luminescence spectra of the mixed complexes [TcClxBr 6–x]2–. *Journal of the Chemical Society, Dalton Transactions, 5*, 921–923. https://doi.org/10.1039/DT9860000921
34. Preetz, W., Peters, G., & Bublitz, D. (1996). Preparation and spectroscopic investigations of mixed octahedral complexes and clusters. *Chemical Reviews, 96*(3), 977–1026. https://doi.org/10.1021/cr940393i
35. Suyver, J. F., Aebischer, A., Biner, D., Gerner, P., Grimm, J., Heer, S., Krämer, K. W., Reinhard, C., & Güdel, H. U. (2005). Novel materials doped with trivalent lanthanides and transition metal ions showing near-infrared to visible photon upconversion. *Optical Materials, 27*(6), 1111–1130. https://doi.org/10.1016/j.optmat.2004.10.021
36. Reber, C., Guedel, H. U., Meyer, G., Schleid, T., & Daul, C. A. (1989). Optical spectroscopic and structural properties of V^{3+}-doped fluoride, chloride, and bromide elpasolite lattices. *Inorganic Chemistry, 28*(16), 3249–3258. https://doi.org/10.1021/ic00315a034
37. Jacobsen, S. M., & Güdel, H. U. (1989). Higher excited state luminescence in Ti^{2+}:$MgCl_2$ Dynamics of radiative and nonradiative processes. *Journal of Luminescence, 43*(3), 125–137. https://doi.org/10.1016/0022-2313(89)90009-4
38. Wenger, O. S., & Güdel, H. U. (2001). Dual luminescence and excited-state dynamics in Ti^{2+} doped NaCl. *The Journal of Physical Chemistry B, 105*(19), 4181–4187. https://doi.org/10.1021/jp004183n
39. Flint, C. D., & Paulusz, A. G. (1981). Infrared and visible luminescence spectra of MoCl63- and MoBr 63- in cubic elpasolite crystals. *Molecular Physics, 44*(4), 925–938. https://doi.org/10.1080/00268978100102891
40. Flint, C. D., & Paulusz, A. G. (1980). High resolution infrared and visible luminescence spectra of OsCl62- and OsBr 62- in cubic crystals. *Molecular Physics, 41*(4), 907–923. https://doi.org/10.1080/00268978000103241

41. Ji, H., Hou, X., Molokeev, M. S., Ueda, J., Tanabe, S., Brik, M. G., Zhang, Z., Wang, Y., & Chen, D. (2020). Ultrabroadband red luminescence of Mn^{4+} in $MgAl_2O_4$ peaking at 651 nm. *Dalton Transactions, 49*(17), 5711–5721. https://doi.org/10.1039/D0DT00931H
42. Harris, J. P., Reber, C., Colmer, H. E., Jackson, T. A., Forshaw, A. P., Smith, J. M., Kinney, R. A., & Telser, J. (2017). Near-infrared $^2E_g \rightarrow ^4A_{2g}$ and visible LMCT luminescence from a molecular bis-(tris(carbene)borate) manganese(IV) complex. *Canadian Journal of Chemistry, 95*(5), 547–552. https://doi.org/10.1139/cjc-2016-0607
43. Harris, J. P., Reber, C., Colmer, H. E., Jackson, T. A., Forshaw, A. P., Smith, J. M., Kinney, R. A., & Telser, J. (2020). Correction: Near-infrared $^2E_g \rightarrow ^4A_{2g}$ and visible LMCT luminescence from a molecular bis-(tris(carbene)borate) manganese(IV) complex. *Canadian Journal of Chemistry, 98*(5), 250. https://doi.org/10.1139/cjc-2020-0119
44. Bussiére, G., Beaulac, R., Cardinal-David, B., & Reber, C. (2001). Coupled electronic states in trans-$MCl_2(H_2O)_4^{n+}$ complexes (M: Ni^{2+}, Co^{2+}, V^{3+}, Cr^{3+}) probed by absorption and luminescence spectroscopy. *Coordination Chemistry Reviews, 219–221*, 509–543. https://doi.org/10.1016/S0010-8545(01)00349-6
45. Atanasov, M., Andreici Eftimie, E.-L., Avram, N. M., Brik, M. G., & Neese, F. (2021). First-principles study of optical absorption energies, ligand field and spin-hamiltonian parameters of Cr^{3+} ions in emeralds. *Inorganic Chemistry*. https://doi.org/10.1021/acs.inorgchem.1c02650
46. Wenger, O. S., Bénard, S., & Güdel, H. U. (2002). Crystal field effects on the optical absorption and luminescence properties of Ni^{2+}-doped chlorides and bromides: Crossover in the emitting higher excited state. *Inorganic Chemistry, 41*(23), 5968–5977. https://doi.org/10.1021/ic020347y
47. Monteiro, J. H. S. K. (2020). Recent advances in luminescence imaging of biological systems using lanthanide(III) luminescent complexes. *Molecules*. https://doi.org/10.3390/molecules25092089
48. Yuan, J., & Wang, G. (2006). Lanthanide-based luminescence probes and time-resolved luminescence bioassays. *Trends Analyt. Chem., 25*(5), 490–500. https://doi.org/10.1016/j.trac.2005.11.013
49. Wei, C., Ma, L., Wei, H., Liu, Z., Bian, Z., & Huang, C. (2018). Advances in luminescent lanthanide complexes and applications. *Science China Technological Science, 61*(9), 1265–1285. https://doi.org/10.1007/s11431-017-9212-7
50. Lever, A. B. P. (1968). *Inorganic electronic spectroscopy* (1st ed.). Elsevier.
51. Ballhausen, C. J. (1962). *Introduction to ligand field theory*. McGraw-Hill Book Company.
52. Tanabe, Y., & Sugano, S. (1954). On the absorption spectra of complex ions I. *Journal of the Physical Society of Japan, 9*(5), 753–766. https://doi.org/10.1143/jpsj.9.753
53. Tanabe, Y., & Sugano, S. (1954). On the absorption spectra of complex ions II. *Journal of the Physical Society of Japan, 9*(5), 766–779. https://doi.org/10.1143/JPSJ.9.766
54. Figgis, B. N., & Hitchman, M. A. (2000). *Ligand field theory and its applications*. Wiley-VCH.
55. Zare, D., Doistau, B., Nozary, H., Besnard, C., Guénée, L., Suffren, Y., Pelé, A.-L., Hauser, A., & Piguet, C. (2017). Cr^{III} as an alternative to Ru^{II} in metallo-supramolecular chemistry. *Dalton Transactions, 46*(28), 8992–9009. https://doi.org/10.1039/c7dt01747b
56. Otto, S., Dorn, M., Förster, C., Bauer, M., Seitz, M., & Heinze, K. (2018). Understanding and exploiting long-lived near-infrared emission of a molecular ruby. *Coordination Chemistry Reviews, 359*, 102–111. https://doi.org/10.1016/j.ccr.2018.01.004
57. Jørgensen, C. K. (1963). Spectroscopy of transition-group complexes. In: *Advances in chemical physics,* (pp. 33–146). Wiley. https://doi.org/10.1002/9780470143513.ch2.
58. Oppenheim, J. & Miller, J. (2021), *Tanabe-Sugano for Mathematica.* Retrieved December 07, 2021, from https://github.com/JulesOpp/Tanabe-Sugano. Accessed 07 Dec 2021
59. Kaufhold, S., & Wärnmark, K. (2020). Design and synthesis of photoactive iron N-heterocyclic carbene complexes. *Catalysts, 10*(1), 132. https://doi.org/10.3390/catal10010132
60. Tang, Y., Zhao, S., Long, B., Liu, J.-C., & Li, J. (2016). On the nature of support effects of metal dioxides MO_2 (M = Ti, Zr, Hf, Ce, Th) in single-atom gold catalysts: importance of quantum primogenic effect. *Journal of Physical Chemistry C, 120*(31), 17514–17526. https://doi.org/10.1021/acs.jpcc.6b05338
61. McCusker, J. K. (2019). Electronic structure in the transition metal block and its implications for light harvesting. *Science, 363*(6426), 484–488. https://doi.org/10.1126/science.aav9104
62. Dorn, M., Kalmbach, J., Boden, P., Päpcke, A., Gómez, S., Förster, C., Kuczelinis, F., Carrella, L. M., Büldt, L. A., Bings, N. H., Rentschler, E., Lochbrunner, S., González, L., Gerhards, M., Seitz, M., & Heinze, K. (2020). A vanadium(III) complex with blue and NIR-II spin-flip luminescence in solution. *Journal of the American Chemical Society, 142*(17), 7947–7955. https://doi.org/10.1021/jacs.0c02122
63. Kirk, A. D., & Porter, G. B. (1980). Luminescence of chromium(III) complexes. *Journal of Physical Chemistry, 84*(8), 887–891. https://doi.org/10.1021/j100445a020
64. Jiménez, J.-R., Doistau, B., Besnard, C., & Piguet, C. (2018). Versatile heteroleptic bis-terdentate Cr(III) chromophores displaying room temperature millisecond excited state lifetimes. *Chemical Communications, 54*(94), 13228–13231. https://doi.org/10.1039/c8cc07671e
65. Whuler, A., Brouty, C., Spinat, P. & Herpin, P. (1977). Structure du complexe actif hydraté (+)-$Cr(en)_3Cl_3 \cdot 2H_2O$. Etude de la configuration absolue et du désordre conformationnel, *Acta Crystallogr. B Struct. Sci.,* **33**(9), 2877–2885. https://doi.org/10.1107/S0567740877009674.
66. Ando, H., Iuchi, S., & Sato, H. (2012). Theoretical study on ultrafast intersystem crossing of chromium(III) acetylacetonate. *Chemical Physics Letters, 535*, 177–181. https://doi.org/10.1016/j.cplett.2012.03.043
67. Penfold, T. J., Gindensperger, E., Daniel, C., & Marian, C. M. (2018). Spin-vibronic mechanism for intersystem crossing. *Chemical Reviews, 118*(15), 6975–7025. https://doi.org/10.1021/acs.chemrev.7b00617
68. Juban, E. A., & McCusker, J. K. (2005). Ultrafast dynamics of ^2E state formation in $Cr(acac)_3$. *Journal of the American Chemical Society, 127*(18), 6857–6865. https://doi.org/10.1021/ja042153i
69. Ballardini, R., Varani, G., Wasgestian, H. F., Moggi, L., & Balzani, V. (1973). Role of the excited states in the photochemical and photophysical behavior of tris(ethylenediamine) chromium(III) in aqueous solutions. *Journal of Physical Chemistry, 77*(25), 2947–2951. https://doi.org/10.1021/j100643a004
70. Adamson, A. W. (1967). Photochemistry of complex ions. IV. Role of quartet excited states in the photochemistry of chromium(III) complexes. *The Journal of Physical Chemistry, 71*(4), 798–808. https://doi.org/10.1021/j100863a003
71. Knochenmuss, R., Reber, C., Rajasekharan, M. V., & Güdel, H. U. (1986). Broadband near-infrared luminescence of Cr^{+3} in the elpasolite lattices $Cs_2NaInCl_6$, $Cs2_NaYCl6$, and $Cs2_NaYBr\ _6$. *The Journal of Chemical Physics, 85*(8), 4280–4289. https://doi.org/10.1063/1.451801
72. Otto, S., Harris, J. P., Heinze, K., & Reber, C. (2018). Molecular ruby under pressure. *Angewandte Chemie International Edition, 57*(34), 11069–11073. https://doi.org/10.1002/anie.201806755

73. Reichenauer, F., Wang, C., Förster, C., Boden, P., Ugur, N., Báez-Cruz, R., Kalmbach, J., Carrella, L. M., Rentschler, E., Ramanan, C., Niedner-Schatteburg, G., Gerhards, M., Seitz, M., Resch-Genger, U., & Heinze, K. (2021). Strongly red-emissive molecular ruby Cr(bpmp)$_2^{3+}$ surpasses Ru(bpy)$_3^{2+}$. *Journal of the American Chemical Society, 143*(30), 11843–11855. https://doi.org/10.1021/jacs.1c05971

74. Otto, S., Nauth, A. M., Ermilov, E., Scholz, N., Friedrich, A., Resch-Genger, U., Lochbrunner, S., Opatz, T., & Heinze, K. (2017). Photo-chromium: sensitizer for visible-light-induced oxidative C−H bond functionalization-electron or energy transfer? *ChemPhotoChem, 1*(8), 344–349. https://doi.org/10.1002/cptc.201700077

75. Fukuda, R., Walters, R. T., Macke, H., & Adamson, A. W. (1979). Rate of primary photoproduct formation for aqueous tris(ethylenediamine)chromium(3+) and chloropentaammine-chromium(2+). *Journal of Physical Chemistry, 83*(16), 2097–2103. https://doi.org/10.1021/j100479a009

76. Barbour, J. C., Kim, A. J. I., deVries, E., Shaner, S. E., & Lovaasen, B. M. (2017). Chromium(III) bis-arylterpyridyl complexes with enhanced visible absorption via incorporation of intraligand charge-transfer transitions. *Inorganic Chemistry, 56*(14), 8212–8222. https://doi.org/10.1021/acs.inorgchem.7b00953

77. Yardley, J. T., & Beattie, J. K. (1972). Lifetime of the $^4T_{2g}$ state of tris(2,4-pentanedionato)chromium(III) reexamined. *Journal of the American Chemical Society, 94*(25), 8925–8926. https://doi.org/10.1021/ja00780a057

78. Treiling, S., Wang, C., Förster, C., Reichenauer, F., Kalmbach, J., Boden, P., Harris, J. P., Carrella, L. M., Rentschler, E., Resch-Genger, U., Reber, C., Seitz, M., Gerhards, M., & Heinze, K. (2019). Luminescence and light-driven energy and electron transfer from an exceptionally long-lived excited state of a non-innocent chromium(III) complex. *Angewandte Chemie International Edition, 58*(50), 18075–18085. https://doi.org/10.1002/anie.201909325

79. Wang, C., Otto, S., Dorn, M., Kreidt, E., Lebon, J., Sršan, L., Di Martino-Fumo, P., Gerhards, M., Resch-Genger, U., Seitz, M., & Heinze, K. (2018). Deuterated molecular ruby with record luminescence quantum yield. *Angewandte Chemie International Edition, 57*(4), 1112–1116. https://doi.org/10.1002/anie.201711350

80. Chen, S.-N., & Porter, G. B. (1970). Lifetime of the $^4T_{2g}$ state of chromium(III) complexes. *Journal of the American Chemical Society, 92*(7), 2189–2190. https://doi.org/10.1021/ja00710a096

81. Barker, K. D., Barnett, K. A., Connell, S. M., Glaeser, J. W., Wallace, A. J., Wildsmith, J., Herbert, B. J., Wheeler, J. F., & Kane-Maguire, N. A. P. (2001). Synthesis and characterization of heteroleptic Cr(diimine)$_3^{3+}$ complexes. *Inorganica Chimica Acta, 316*(1–2), 41–49. https://doi.org/10.1016/S0020-1693(01)00377-2

82. McDaniel, A. M., Tseng, H.-W., Damrauer, N. H., & Shores, M. P. (2010). Synthesis and solution phase characterization of strongly photooxidizing heteroleptic Cr(III) tris-dipyridyl complexes. *Inorganic Chemistry, 49*(17), 7981–7991. https://doi.org/10.1021/ic1009972

83. Serpone, N., Jamieson, M. A., Henry, M. S., Hoffman, M. Z., Bolletta, F., & Maestri, M. (1979). Excited-state behavior of polypyridyl complexes of chromium(III). *Journal of the American Chemical Society, 101*, 2907–2916. https://doi.org/10.1021/ja00505a019

84. Perkovic, M. W., Heeg, M. J., & Endicott, J. F. (1991). Stereochemical perturbations of the relaxation behavior of (2E) chromium(III). Ground-state x-ray crystal structure, photophysics, and molecular mechanics simulations of the quasi-cage complex [4,4',4"-ethylidynetris(3-azabutan-1-amine)]chromium tribromide. *Inorganic Chemistry, 30*(16), 3140–3147. https://doi.org/10.1021/ic00016a009

85. Otto, S., Förster, C., Wang, C., Resch-Genger, U., & Heinze, K. (2018). A strongly luminescent chromium(III) complex acid. *Chemistry--A European Journal, 24*(48), 12555–12563. https://doi.org/10.1002/chem.201802797

86. Higgins, R. F., Fatur, S. M., Shepard, S. G., Stevenson, S. M., Boston, D. J., Ferreira, E. M., Damrauer, N. H., Rappé, A. K., & Shores, M. P. (2016). Uncovering the roles of oxygen in Cr(III) photoredox catalysis. *Journal of the American Chemical Society, 138*(16), 5451–5464. https://doi.org/10.1021/jacs.6b02723

87. Sinha, N., Jiménez, J.-R., Pfund, B., Prescimone, A., Piguet, C., & Wenger, O. S. (2021). A near-infrared-II emissive chromium(III) complex. *Angewandte Chemie (International ed. in English), 60*(44), 23722–23728. https://doi.org/10.1002/anie.202106398

88. Stein, L., Boden, P., Naumann, R., Förster, C., Niedner Schatteburg, G., & Heinze, K. (2022). The overlooked NIR luminescence of the Ir(ppy)$_3$ analogue Cr(ppy)$_3$. *Chemical Communications*. https://doi.org/10.1039/D2CC00680D

89. Dill, R. D., Portillo, R. I., Shepard, S. G., Shores, M. P., Rappé, A. K., & Damrauer, N. H. (2020). Long-lived mixed ^{2}MLCT/MC states in antiferromagnetically coupled d^3 vanadium(II) bipyridine and phenanthroline complexes. *Inorganic Chemistry, 59*(20), 14706–14715. https://doi.org/10.1021/acs.inorgchem.0c01950

90. Laporte, O., & Meggers, W. F. (1925). Some rules of spectral structure. *Journal of the Optical Society of America, 11*(5), 459. https://doi.org/10.1364/JOSA.11.000459

91. Dannöhl-Fickler, R., Kelm, H., & Wasgestian, F. (1975). Solvent and temperature dependence of the phosphorescence decay time of hexacyanochromate(III). *Journal of Luminescence, 10*(2), 103–112. https://doi.org/10.1016/0022-2313(75)90038-1

92. McDaniel, A. M., Tseng, H.-W., Hill, E. A., Damrauer, N. H., Rappé, A. K., & Shores, M. P. (2013). Syntheses and photophysical investigations of Cr(III) hexadentate iminopyridine complexes and their tris(bidentate) analogues. *Inorganic Chemistry, 52*(3), 1368–1378. https://doi.org/10.1021/ic302055r

93. Xiang, H., Cheng, J., Ma, X., Zhou, X., & Chruma, J. J. (2013). Near-infrared phosphorescence: Materials and applications. *Chemical Society Reviews, 42*(14), 6128–6185. https://doi.org/10.1039/c3cs60029g

94. Scattergood, P. A. (2020). Recent advances in chromium coordination chemistry: luminescent materials and photocatalysis. In N. J. Patmore & P. I. P. Elliott (Eds.), *Organometallic chemistry* (pp. 1–34). Royal Society of Chemistry. https://doi.org/10.1039/9781788017077-00001

95. Kreidt, E., Kruck, C., & Seitz, M. (2018). Nonradiative deactivation of lanthanoid luminescence by multiphonon relaxation in molecular complexes. In J.-C.G. Bünzli, V. K. Pecharsky, G.-Y. Adachi, K. A. Gschneidner, & E. LeRoy (Eds.), *Handbook on the physics and chemistry of rare earths* (pp. 35–79). Amsterdam, Oxford: North-Holland. https://doi.org/10.1016/bs.hpcre.2018.04.001

96. Henry, M. S. (1977). Prolongation of the lifetime of the ^{2}E state of tris(2,2'-bipyridine)chromium(III) ion by anions in aqueous solution. *Journal of the American Chemical Society, 99*(18), 6138–6139. https://doi.org/10.1021/ja00460a068

97. Henry, M. S., & Hoffman, M. Z. (1978). Solution medium effects on the photophysics and photochemistry of polypyridyl complexes of chromium(III). In M. S. Wrighton (Ed.), *Inorganic and organometallic photochemistry* (pp. 91–114). American Chemical Society. https://doi.org/10.1021/ba-1978-0168.ch006

98. Wasgestian, H. F., Ballardini, R., Varani, G., Moggi, L., & Balzani, V. (1973). Quenching of the tris(ethylenediamine) chromium(III) phosphorescence by some transition metal ions

in aqueous solutions. *Journal of Physical Chemistry, 77*(22), 2614–2617. https://doi.org/10.1021/j100640a007

99. Basu, U., Otto, S., Heinze, K., & Gasser, G. (2019). Biological evaluation of the NIR-emissive ruby analogue $[Cr(ddpd)_2][BF_4]_3$ as a photodynamic therapy photosensitizer. *European Journal of Inorganic Chemistry, 2019*(1), 37–41. https://doi.org/10.1002/ejic.201801023
100. Wang, C., Kitzmann, W. R., Weigert, F., Förster, C., Wang, X., Heinze, K., & Resch-Genger, U. (2022). Matrix effects on photoluminescence and oxygen sensitivity of a molecular ruby. *ChemPhotoChem*. https://doi.org/10.1002/cptc.202100296
101. Luo, L.-J., Su, Q.-Q., Cheng, S.-C., Xiang, J., Man, W.-L., Shu, W.-M., Zeng, M.-H., Yiu, S.-M., Ko, C.-C., & Lau, T.-C. (2020). Tunable luminescent properties of tricyanoosmium nitrido complexes bearing a chelating O^N ligand. *Inorganic Chemistry, 59*(7), 4406–4413. https://doi.org/10.1021/acs.inorgchem.9b03554
102. Coppo, P., Plummer, E. A., & de Cola, L. (2004). Tuning iridium(III) phenylpyridine complexes in the "almost blue" region. *Chemical Communications, 15*, 1774–1775. https://doi.org/10.1039/b406851c
103. Duvenhage, M. M., Visser, H. G., Ntwaeaborwa, O. M., & Swart, H. C. (2014). The effect of electron donating and withdrawing groups on the morphology and optical properties of Alq_3. *Physica B: Condens Matter, 439*, 46–49. https://doi.org/10.1016/j.physb.2013.11.049
104. Chatterjee, K. K., & Forster, L. S. (1964). Electronic transitions in chromium(III) complexes—IV radiative and non-radiative transition probabilities. *Spectrochimica Acta, 20*(10), 1603–1609. https://doi.org/10.1016/0371-1951(64)80139-9
105. Witzke, H. (1971). Semi-empirical evaluations of the Racah B and C parameters from the crystal field spectra of chromium(III) complexes. *Theoretica Chimica Acta, 20*(2), 171–185. https://doi.org/10.1007/BF00569263
106. Stevenson, S. M., Shores, M. P., & Ferreira, E. M. (2015). Photooxidizing chromium catalysts for promoting radical cation cycloadditions. *Angewandte Chemie International Edition, 54*(22), 6506–6510. https://doi.org/10.1002/anie.201501220
107. Yang, Y., Liu, Q., Zhang, L., Yu, H., & Dang, Z. (2017). Mechanistic investigation on oxygen-mediated photoredox diels-alder reactions with chromium catalysts. *Organometallics, 36*(3), 687–698. https://doi.org/10.1021/acs.organomet.6b00886
108. Otto, S., Scholz, N., Behnke, T., Resch-Genger, U., & Heinze, K. (2017). Thermo-chromium: A contactless optical molecular thermometer. *Chemistry--A European Journal, 23*(50), 12131–12135. https://doi.org/10.1002/chem.201701726
109. Wang, C., Otto, S., Dorn, M., Heinze, K., & Resch-Genger, U. (2019). Luminescent TOP nanosensors for simultaneously measuring temperature, oxygen, and pH at a single excitation wavelength. *Analytical Chemistry, 91*(3), 2337–2344. https://doi.org/10.1021/acs.analchem.8b05060
110. Forman, R. A., Piermarini, G. J., Barnett, J. D., & Block, S. (1972). Pressure measurement made by the utilization of ruby sharp-line luminescence. *Science, 176*(4032), 284–285. https://doi.org/10.1126/science.176.4032.284
111. Chijioke, A. D., Nellis, W. J., Soldatov, A., & Silvera, I. F. (2005). The ruby pressure standard to 150GPa. *Journal of Applied Physics, 98*(11), 114905. https://doi.org/10.1063/1.2135877
112. Reber, C., Grey, J. K., Lanthier, E., & Frantzen, K. A. (2011). Pressure-induced change of d-d luminescence energies, vibronic structure and band intensities in transition metal complexes. In J. P. Fackler & L. Falvello (Eds.), *Techniques in inorganic chemistry* (pp. 233–254). Taylor & Francis. https://doi.org/10.1080/02603590500403909
113. Wang, C., Reichenauer, F., Kitzmann, W. R., Kerzig, C., Heinze, K. & Resch-Genger, U. (2021). Efficient Triplet-Triplet Annihilation Upconversion Sensitized by a Second-Generation Molecular Ruby via an Underexplored Energy Transfer Mechanism, *submitted*.
114. Imbert, D., Cantuel, M., Bünzli, J.-C.G., Bernardinelli, G., & Piguet, C. (2003). Extending lifetimes of lanthanide-based near-infrared emitters (Nd, Yb) in the millisecond range through Cr(III) sensitization in discrete bimetallic edifices. *Journal of the American Chemical Society, 125*(51), 15698–15699. https://doi.org/10.1021/ja0386501
115. Aboshyan-Sorgho, L., Nozary, H., Aebischer, A., Bünzli, J.-C.G., Morgantini, P.-Y., Kittilstved, K. R., Hauser, A., Eliseeva, S. V., Petoud, S., & Piguet, C. (2012). Optimizing millisecond time scale near-infrared emission in polynuclear chrome(III)-lanthanide(III) complexes. *Journal of the American Chemical Society, 134*(30), 12675–12684. https://doi.org/10.1021/ja304009b
116. Aboshyan-Sorgho, L., Besnard, C., Pattison, P., Kittilstved, K. R., Aebischer, A., Bünzli, J.-C.G., Hauser, A., & Piguet, C. (2011). Near-infrared→visible light upconversion in a molecular trinuclear d-f-d complex. *Angewandte Chemie International Edition, 50*(18), 4108–4112. https://doi.org/10.1002/anie.201100095
117. Kalmbach, J., Wang, C., You, Y., Förster, C., Schubert, H., Heinze, K., Resch-Genger, U., & Seitz, M. (2020). Near-IR to near-IR upconversion luminescence in molecular chromium ytterbium salts. *Angewandte Chemie International Edition, 59*(42), 18804–18808. https://doi.org/10.1002/anie.202007200
118. Bünzli, J.-C.G., & Eliseeva, S. V. (2010). Lanthanide NIR luminescence for telecommunications, bioanalyses and solar energy conversion. *Journal of Rare Earths, 28*(6), 824–842. https://doi.org/10.1016/S1002-0721(09)60208-8
119. MacKenzie, L. E., & Pal, R. (2021). Circularly polarized lanthanide luminescence for advanced security inks. *Nature Reviews Chemistry, 5*(2), 109–124. https://doi.org/10.1038/s41570-020-00235-4
120. Hao, C., Xu, L., Sun, M., Zhang, H., Kuang, H., & Xu, C. (2019). Circularly polarized light triggers biosensing based on chiral assemblies. *Chemistry--A European Journal, 25*(53), 12235–12240. https://doi.org/10.1002/chem.201901721
121. Zinna, F., & Di Bari, L. (2015). Lanthanide circularly polarized luminescence: Bases and applications. *Chirality, 27*(1), 1–13. https://doi.org/10.1002/chir.22382
122. Dee, C., Zinna, F., Kitzmann, W. R., Pescitelli, G., Heinze, K., Di Bari, L., & Seitz, M. (2019). Strong circularly polarized luminescence of an octahedral chromium(III) complex. *Chemical Communications, 55*(87), 13078–13081. https://doi.org/10.1039/c9cc06909g
123. Poncet, M., Benchohra, A., Jiménez, J.-R., & Piguet, C. (2021). Chiral chromium(III) complexes as promising candidates for circularly polarized luminescence. *ChemPhotoChem, 5*(10), 880–892. https://doi.org/10.1002/cptc.202100146
124. Doistau, B., Jiménez, J.-R., & Piguet, C. (2020). Beyond chiral organic (p-Block) chromophores for circularly polarized luminescence: The success of d-block and f-block chiral complexes. *Frontiers in Chemistry, 8*, 555. https://doi.org/10.3389/fchem.2020.00555
125. Kreidt, E., Arrico, L., Zinna, F., Di Bari, L., & Seitz, M. (2018). Circularly polarised luminescence in enantiopure samarium and europium cryptates. *Chemistry--A European Journal, 24*(51), 13556–13564. https://doi.org/10.1002/chem.201802196
126. Arrico, L., Di Bari, L., & Zinna, F. (2021). Quantifying the overall efficiency of circularly polarized emitters. *Chemistry--A European Journal, 27*(9), 2920–2934. https://doi.org/10.1002/chem.202002791
127. Fataftah, M. S., Zadrozny, J. M., Coste, S. C., Graham, M. J., Rogers, D. M., & Freedman, D. E. (2016). Employing forbidden transitions as qubits in a nuclear spin-free chromium complex.

Journal of the American Chemical Society, 138(4), 1344–1348. https://doi.org/10.1021/jacs.5b11802

128. Fataftah, M. S., Bayliss, S. L., Laorenza, D. W., Wang, X., Phelan, B. T., Wilson, C. B., Mintun, P. J., Kovos, B. D., Wasielewski, M. R., Han, S., Sherwin, M. S., Awschalom, D. D., & Freedman, D. E. (2020). Trigonal bipyramidal V^{3+} complex as an optically addressable molecular qubit candidate. *Journal of the American Chemical Society, 142*, 20400–20408. https://doi.org/10.1021/jacs.0c08986
129. Wojnar, M. K., Laorenza, D. W., Schaller, R. D., & Freedman, D. E. (2020). Nickel(II) metal complexes as optically addressable qubit candidates. *Journal of the American Chemical Society, 142*(35), 14826–14830. https://doi.org/10.1021/jacs.0c06909
130. Bayliss, S. L., Laorenza, D. W., Mintun, P. J., Kovos, B. D., Freedman, D. E., & Awschalom, D. D. (2020). Optically addressable molecular spins for quantum information processing. *Science, 370*(6522), 1309–1312. https://doi.org/10.1126/science.abb9352
131. Laorenza, D. W., Kairalapova, A., Bayliss, S. L., Goldzak, T., Greene, S. M., Weiss, L. R., Deb, P., Mintun, P. J., Collins, K. A., Awschalom, D. D., Berkelbach, T. C., & Freedman, D. E. (2021). Tunable Cr^{4+} molecular color centers. *Journal of the American Chemical Society*. https://doi.org/10.1021/jacs.1c10145
132. Lenz, S., Bamberger, H., Hallmen, P. P., Thiebes, Y., Otto, S., Heinze, K., & van Slageren, J. (2019). Chromium(III)-based potential molecular quantum bits with long coherence times. *Physical Chemistry Chemical Physics: PCCP, 21*(13), 6976–6983. https://doi.org/10.1039/C9CP00745H
133. Wijeratne, G. B., Zolnhofer, E. M., Fortier, S., Grant, L. N., Carroll, P. J., Chen, C.-H., Meyer, K., Krzystek, J., Ozarowski, A., Jackson, T. A., Mindiola, D. J., & Telser, J. (2015). Electronic structure and reactivity of a well-defined mononuclear complex of Ti(II). *Inorganic Chemistry, 54*(21), 10380–10397. https://doi.org/10.1021/acs.inorgchem.5b01796
134. Reinholdt, A., Pividori, D., Laughlin, A. L., DiMucci, I. M., MacMillan, S. N., Jafari, M. G., Gau, M. R., Carroll, P. J., Krzystek, J., Ozarowski, A., Telser, J., Lancaster, K. M., Meyer, K., & Mindiola, D. J. (2020). A mononuclear and high-spin tetrahedral Ti^{II} complex. *Inorganic Chemistry, 59*(24), 17834–17850. https://doi.org/10.1021/acs.inorgchem.0c02586
135. Jensen, J. A., Wilson, S. R., Schultz, A. J., & Girolami, G. S. (1987). Divalent titanium chemistry. Synthesis, reactivity, and x-ray and neutron diffraction studies of Ti(BH4)2(dmpe)2 and Ti(CH3)2(dmpe)2. *Journal of the American Chemical Society, 109*(26), 8094–8096. https://doi.org/10.1021/ja00260a029
136. Beaumier, E. P., Pearce, A. J., See, X. Y., & Tonks, I. A. (2019). Modern applications of low-valent early transition metals in synthesis and catalysis. *Nature Reviews Chemistry, 3*(1), 15–34. https://doi.org/10.1038/s41570-018-0059-x
137. Araya, M. A., Cotton, F. A., Matonic, J. H., & Murillo, C. A. (1995). An efficient reduction process leading to titanium(II) and niobium(II): Preparation and structural characterization of trans-$MCl_2(py)_4$ compounds, M = Ti, Nb, and Mn. *Inorganic Chemistry, 34*(22), 5424–5428. https://doi.org/10.1021/ic00126a009
138. Fortier, S., & Gomez-Torres, A. (2021). Redox chemistry of discrete low-valent titanium complexes and low-valent titanium synthons. *Chemical Communications, 57*(80), 10292–10316. https://doi.org/10.1039/D1CC02772G
139. Kayal, A., Kuncheria, J., & Lee, S. C. (2001). Bishydrotris(pyrazol-1-yl)boratotitanium(II): A stable Tp_2M complex of singular reactivity. *Chemical Communications, 23*, 2482–2483. https://doi.org/10.1039/B108115B
140. Dingle, R., McCarthy, P. J., & Ballhausen, C. J. (1969). Crystal spectra of hexaurea complexes. III. Optical and magnetic properties of crystals containing the hexaurea vanadium (III) Ion. *The Journal of Chemical Physics, 50*(5), 1957–1962. https://doi.org/10.1063/1.1671314
141. Flint, C. D., & Greenough, P. (1972). Luminescence spectrum of the $V(urea)_6^{3+}$ ion. *Chemical Physics Letters, 16*(2), 369–370. https://doi.org/10.1016/0009-2614(72)80294-X
142. Beaulac, R., Tregenna-Piggott, P. L. W., Barra, A.-L., Weihe, H., Luneau, D., & Reber, C. (2006). The electronic ground state of $V(urea)_6^{3+}$ probed by NIR luminescence, electronic Raman, and high-field EPR spectroscopies. *Inorganic Chemistry, 45*(8), 3399–3407. https://doi.org/10.1021/ic051709f
143. Dorn, M., East, N. R., Förster, C., Kitzmann, W. R., Moll, J., Reichenauer, F., Reuter, T., Stein, L., & Heinze, K. (2022). d-d and charge transfer photochemistry of 3d metal complexes. In J. Reedijk (Ed.), *Comprehensive inorganic chemistry III*. Elsevier.
144. Dorn, M., Kalmbach, J., Boden, P., Kruse, A., Dab, C., Reber, C., Niedner-Schatteburg, G., Lochbrunner, S., Gerhards, M., Seitz, M., & Heinze, K. (2021). Ultrafast and long-time excited state kinetics of an NIR-emissive vanadium(III) complex I: Synthesis, spectroscopy and static quantum chemistry. *Chemical Science, 12*(32), 10780–10790. https://doi.org/10.1039/d1sc02137k
145. Zobel, J. P., Knoll, T., & González, L. (2021). Ultrafast and long-time excited state kinetics of an NIR-emissive vanadium(III) complex II. Elucidating triplet-to-singlet excited-state dynamics. *Chemica Science, 12*(32), 10791–10801. https://doi.org/10.1039/d1sc02149d
146. Juban, E. A., Smeigh, A. L., Monat, J. E., & McCusker, J. K. (2006). Ultrafast dynamics of ligand-field excited states. *Coordination Chemistry Reviews, 250*, 1783–1791. https://doi.org/10.1016/J.CCR.2006.02.010
147. Brik, M., Avram, N., & Avram, C. (2005). Crystal field analysis of the ground and excited state absorption of a Cr^{4+} ion in $LiAlO_2$ and $LiGaO_2$ crystals. *Central European Journal of Physics, 3*(4), 508–524. https://doi.org/10.2478/BF02475609
148. Neyhart, G. A., Bakir, M., Boaz, J., Vining, W. J., & Patrick Sullivan, B. (1991). Photophysics and photochemistry of rhenium(V)-nitrogen triple bonds. *Coordination Chemistry Reviews, 111*, 27–32. https://doi.org/10.1016/0010-8545(91)84007-R
149. Savoie, C., & Reber, C. (1998). Emitting state energies and vibronic structure in the luminescence spectra of trans-dioxorhenium(V) complexes. *Coordination Chemistry Reviews, 171*, 387–398. https://doi.org/10.1016/S0010-8545(98)90059-5
150. Yam, V.W.-W., & Che, C.-M. (1990). Photochemistry and photophysics of trans-d^2-dioxo complexes of osmium(VI). *Coordination Chemistry Reviews, 97*, 93–104. https://doi.org/10.1016/0010-8545(90)80082-5
151. Ikeda, H., Ito, A., Sakuda, E., Kitamura, N., Takayama, T., Sekine, T., Shinohara, A., & Yoshimura, T. (2013). Excited-state characteristics of tetracyanidonitridorhenium(V) and -technetium(V) complexes with N-heteroaromatic ligands. *Inorganic Chemistry, 52*(11), 6319–6327. https://doi.org/10.1021/ic302463v
152. Sasaki, K., Yamate, H., Yoshino, H., Miura, H., Shimoda, Y., Miyata, K., Onda, K., Ohtani, R., & Ohba, M. (2020). Vapor switching of the luminescence mechanism in a Re(V) complex. *Chemical Communications, 56*(85), 12961–12964. https://doi.org/10.1039/D0CC05462C
153. Lanthier, E., Bendix, J., & Reber, C. (2010). Pressure-dependent luminescence spectroscopy of molybdenum(IV) oxo complexes. *Dalton Transactions, 39*(15), 3695–3705. https://doi.org/10.1039/b924242b
154. Isovitsch, R. A., Beadle, A. S., Fronczek, F. R., & Maverick, A. W. (1998). Electronic absorption spectra and phosphorescence of oxygen-containing molybdenum(IV) complexes. *Inorganic Chemistry, 37*(17), 4258–4264. https://doi.org/10.1021/ic971186e

155. Kirk, A. D. (1981). Chromium(III) photochemistry and photophysics. *Coordination Chemistry Reviews, 39*(1–2), 225–263. https://doi.org/10.1016/s0010-8545(00)80515-9
156. Forster, L. S. (1990). The photophysics of chromium(III) complexes. *Chemical Reviews, 90*(2), 331–353. https://doi.org/10.1021/cr00100a001
157. Kjær, K. S., van Driel, T. B., Harlang, T. C. B., Kunnus, K., Biasin, E., Ledbetter, K., Hartsock, R. W., Reinhard, M. E., Koroidov, S., Li, L., Laursen, M. G., Hansen, F. B., Vester, P., Christensen, M., Haldrup, K., Nielsen, M. M., Dohn, A. O., Pápai, M. I., Møller, K. B., … Gaffney, K. J. (2019). Finding intersections between electronic excited state potential energy surfaces with simultaneous ultrafast X-ray scattering and spectroscopy. *Chemical Science, 10*(22), 5749–5760. https://doi.org/10.1039/c8sc04023k
158. Wegeberg, C., & Wenger, O. S. (2021). Luminescent first-row transition metal complexes. *JACS Au*. https://doi.org/10.1021/jacsau.1c00353
159. Schläfer, H., Gausmann, H., & Witzke, H. (1966). Phosphorescence of molybdenum (III) complexes. *Journal of Molecular Spectroscopy, 21*(1–4), 125–129. https://doi.org/10.1016/0022-2852(66)90131-7
160. Yao, Q., & Maverick, A. W. (1988). Near-infrared luminescence of octahedral molybdenum(III) and rhenium(IV) complexes in solution. *Inorganic Chemistry, 27*(10), 1669–1670. https://doi.org/10.1021/ic00283a001
161. Mohammed, A. K., Isovitsch, R. A., & Maverick, A. W. (1998). Solution photophysics, one-electron photooxidation, and photoinitiated two-electron oxidation of molybdenum(III) complexes. *Inorganic Chemistry, 37*(11), 2779–2785. https://doi.org/10.1021/ic970955r
162. Cornioley-Deuschel, C., & von Zelewsky, A. (1987). Stability of d3 diimine complexes: molybdenum(III) vs chromium(III). *Inorganic Chemistry, 26*(6), 962–963. https://doi.org/10.1021/ic00253a040
163. Stiefel, E. I. (1977). The coordination and bioinorganic chemistry of molybdenum. In S. J. Lippard (Ed.), *Progress in inorganic chemistry* (pp. 1–223). Wiley. https://doi.org/10.1002/9780470166239.ch1
164. Young, C. G. (2004). Molybdenum. In J. A. McCleverty & T. J. Meyer (Eds.), *Comprehensive coordination chemistry II* (pp. 415–527). Elsevier/Pergamon. https://doi.org/10.1016/B0-08-043748-6/03033-4
165. Dunn, T. M. (1961). Spin-orbit coupling in the first and second transition series. *Transactions of the Faraday Society, 57*, 1441. https://doi.org/10.1039/TF9615701441
166. Koseki, S., Matsunaga, N., Asada, T., Schmidt, M. W., & Gordon, M. S. (2019). Spin-orbit coupling constants in atoms and ions of transition elements: comparison of effective core potentials, model core potentials, and all-electron methods. *Journal of Physical Chemistry A, 123*(12), 2325–2339. https://doi.org/10.1021/acs.jpca.8b09218
167. Morrison, C. A. (1992). *Crystal fields for transition-metal ions in laser host materials*. Springer.
168. Fleischauer, P. D., & Fleischauer, P. (1970). Photoluminescence of transition metal coordination compounds. *Chemical Reviews, 70*(2), 199–230. https://doi.org/10.1021/cr60264a002
169. Sartori, G., Cervone, E., & Cancellieri, P. (1963). The electronic structure of d^3 complexes using ligand field theory. *Atti della Accademia Nazionale dei Lincei, Classe di Scienze Fisiche, Matematiche e Naturali, 35*, 226.
170. Maverick, A. W., Lord, M. D., Yao, Q., & Henderson, L. J. (1991). Photophysics and photochemistry of hexachlororhenate(IV) and hexabromorhenate(IV). *Inorganic Chemistry, 30*(3), 553–558. https://doi.org/10.1021/ic00003a040
171. Holleman, A. F., & Wiberg, N. (2017). *Hollemann Wiberg, Grundlagen und Hauptgruppenelemente, Band 1* (103rd ed.). De Gruyter.
172. Fujita, I., Yazaki, T., Torii, Y., & Kobayashi, H. (1972). Electronic absorption spectra of tris(2,2′-bipyridine)- and Tris(1,10-phenanthroline) complexes of Vanadium(II) and Chromium(II). *Bulletin Chemical Society of Japan, 45*(7), 2156–2161. https://doi.org/10.1246/bcsj.45.2156
173. Joyce, J. P., Portillo, R. I., Nite, C. M., Nite, J. M., Nguyen, M. P., Rappé, A. K., & Shores, M. P. (2021). Electronic structures of Cr(III) and V(II) polypyridyl systems: Undertones in an isoelectronic analogy. *Inorganic Chemistry, 60*(17), 12823–12834. https://doi.org/10.1021/acs.inorgchem.1c01129
174. Kee, T. (1998). Niobium and tantalum 1995. *Coordination Chemistry Reviews, 169*(1), 129–152. https://doi.org/10.1016/S0010-8545(98)00004-6
175. Wexler, P. A., Wigley, D. E., Koerner, J. B., & Albright, T. A. (1991). Preparation, properties, and bonding analysis of tantalum(II) η^6-arene complexes. *Organometallics, 10*(7), 2319–2327. https://doi.org/10.1021/om00053a039
176. Thiyagarajan, B., Michalczyk, L., Bollinger, J. C., & Bruno, J. W. (1996). Generation of organoniobium(II) radicals and synthesis of heterometallic niobium−mercury compounds. *Organometallics, 15*(11), 2588–2590. https://doi.org/10.1021/om960152w
177. Tayebani, M., Gambarotta, S., & Yap, G. (1998). C−H versus C−N bond cleavage promoted by niobium(II) amide. *Organometallics, 17*(17), 3639–3641. https://doi.org/10.1021/om980298q
178. Noh, W., & Girolami, G. S. (2008). Mono(cycloheptatrienyl) tantalum chemistry: Synthesis and characterization of new tantalum halide, hydride, and alkyl species. *Inorganic Chemistry, 47*(22), 10682–10691. https://doi.org/10.1021/ic8015035
179. Cohen, J. L., & Hoggard, P. E. (2009). Photosolvation reactions of hexabromorhenate(IV). *Inorganica Chimica Acta, 362*(2), 580–582. https://doi.org/10.1016/j.ica.2008.03.119
180. McCusker, J. K., Walda, K. N., Dunn, R. C., Simon, J. D., Magde, D., & Hendrickson, D. N. (1993). Subpicosecond ^{1}MLCT -> $^5T_2$ intersystem crossing of low-spin polypyridyl ferrous complexes. *Journal of the American Chemical Society, 115*(1), 298–307. https://doi.org/10.1021/ja00054a043
181. Shari‘atiVura-Weis, Y. J. (2021). Ballistic $\Delta S = 2$ intersystem crossing in a cobalt cubane following ligand-field excitation probed by extreme ultraviolet spectroscopy. *Physical Chemistry Chemical Physics: PCCP*. https://doi.org/10.1039/D1CP04136C
182. Scarborough, C. C., Sproules, S., Doonan, C. J., Hagen, K. S., Weyhermüller, T., & Wieghardt, K. (2012). Scrutinizing low-spin Cr(II) complexes. *Inorganic Chemistry, 51*(12), 6969–6982. https://doi.org/10.1021/ic300882r
183. Eaton, J. P., & Nicholls, D. (1981). The complex cyanides of chromium(II) and chromium(0). *Transition Metal Chemistry, 6*(4), 203–206. https://doi.org/10.1007/BF00618223
184. Becker, P. M., Förster, C., Carrella, L. M., Boden, P., Hunger, D., van Slageren, J., Gerhards, M., Rentschler, E., & Heinze, K. (2020). Spin crossover and long-lived excited states in a reduced molecular ruby. *Chemistry--A European Journal, 26*(32), 7199–7204. https://doi.org/10.1002/chem.202001237
185. Holleman, A. F., & Wiberg, N. (2017). *Hollemann Wiberg, Nebengruppenelemente, Lanthanoide, Actinoide, Transactinoide, Band 2* (103rd ed.). De Gruyter.
186. Cotton, F. A., Eglin, J. L., & Wiesinger, K. J. (1992). Synthesis and characterization of molybdenum species: Dinuclear and mononuclear species of the molecular formulas $[Mo_2(O_2CCH_3)_2(LL)_2][BF_4]_2$ and $[Mo(O)(F)(LL)_2][BF_4]$ where LL=bis-phosphine. The use of $[Mo(NCCH_3)_{10}][BF_4]_4$ as a source for the $[Mo_2]^{4+}$ core. *Inorganica Chimica Acta, 195*, 11–23.

187. Cotton, F. A., & Wiesinger, K. J. (1992). Decakis(Acetonitrile) Dimolybdenum(II) Tetrafluoroborate(1-). *Inorganic Syntheses, 29*, 134–137.
188. Holste, G. (1975). $Mo_2(CH_3COO)_4$, $Mo_2(C_6H_5COO)_4$ und $[Mo_6Cl_8]Cl_2(CH_3COO)_2$. *Zeitschrift für Anorganische und Allgemeine Chemie, 414*(1), 81–90. https://doi.org/10.1002/zaac.19754140111
189. Johnson, K. D., & Powell, G. L. (2008). Microwave-assisted synthesis of dimolybdenum tetracarboxylates and a decanuclear osmium cluster. *Journal of Organometallic Chemistry, 693*(8–9), 1712–1715. https://doi.org/10.1016/j.jorganchem.2007.11.036
190. Maverick, A. W., Najdzionek, J. S., MacKenzie, D., Nocera, D. G., & Gray, H. B. (1983). Spectroscopic, electrochemical, and photochemical properties of molybdenum(II) and tungsten(II) halide clusters. *Journal of the American Chemical Society, 105*(7), 1878–1882. https://doi.org/10.1021/ja00345a034
191. Eltayeb, N. E., Teoh, S. G., Kusrini, E., Adnan, R., & Fun, H. K. (2010). The manganese(III) complex with chelating Schiff base ligand: X-ray structure, spectroscopic and computational studies. *Spectrochimica Acta Part A: Molecular and Biomolecular Spectroscopy, 75*(1), 453–457. https://doi.org/10.1016/j.saa.2009.11.006
192. Majumder, A., Goswami, S., Batten, S. R., Salah El Fallah, M., Ribas, J., & Mitra, S. (2006). Catalytic oxidation of 3,5-di-tert-butylcatechol by a manganese(III) 18-azametallacrown-6 compound: Synthesis, crystal structure, fluorescence, magnetic and kinetic investigation. *Inorganica Chimica Acta, 359*(8), 2375–2382. https://doi.org/10.1016/j.ica.2006.01.045
193. Makarska-Bialokoz, M., Pratviel, G., & St. Radzki. (2008). The influence of solvent polarity on spectroscopic properties of 5-[4-(5-carboxy-1-butoxy)-phenyl]-10,15,20-tris(4-N-methylpyridiniumyl)porphyrin and its complexes with Fe(III) and Mn(III) ions. *Journal of Molecular Structure, 875*(1–3), 468–477. https://doi.org/10.1016/j.molstruc.2007.05.026
194. Sun, E., Shi, Y., Zhang, P., Zhou, M., Zhang, Y., Tang, X., & Shi, T. (2008). Spectroscopic properties and cyclic voltammetry on a series of meso-tetra(p-alkylamidophenyl)porphyrin liquid crystals and their Mn complexes. *Journal of Molecular Structure, 889*(1–3), 28–34. https://doi.org/10.1016/j.molstruc.2008.01.014
195. Abram, U. (2004). Rhenium. In J. A. McCleverty & T. J. Meyer (Eds.), *Comprehensive coordination chemistry II* (pp. 271–402). Elsevier/Pergamon. https://doi.org/10.1016/B0-08-043748-6/04177-3
196. Alberto, R. (2004). Technetium. In J. A. McCleverty & T. J. Meyer (Eds.), *Comprehensive coordination chemistry II* (pp. 127–270). Elsevier/Pergamon. https://doi.org/10.1016/B0-08-043748-6/04022-6
197. Hancock, R. D., & McDougall, G. J. (1977). The role of electronic delocalization over the chelate ring in stabilizing complexes of 2,2′-bipyridyl. *Journal of the Chemical Society Dalton Transactions, 1*, 67–70. https://doi.org/10.1039/dt9770000067
198. Robinson, M. A., Curry, J. D., & Busch, D. H. (1963). Complexes derived from strong field ligands. XVII. Electronic spectra of octahedral Nickel(II) complexes with ligands of the α-diimine and closely related classes. *Inorganic Chemistry, 2*(6), 1178–1181. https://doi.org/10.1021/ic50010a021
199. Henke, W., & Reinen, D. (1977). Spektroskopische Untersuchungen zum Jahn-Teller-Effekt des Cu^{2+}-Ions in Terpyridin-Komplexen $Cu(terpy)_2X_2 \cdot nH2O$ [X = NO, ClO, Br^-]. *Zeitschrift für Anorganische und Allgemeine Chemie, 436*(1), 187–200. https://doi.org/10.1002/zaac.19774360123
200. Dorn, M., Mack, K., Carrella, L. M., Rentschler, E., Förster, C., & Heinze, K. (2018). Structure and electronic properties of an expanded terpyridine complex of Nickel(II) $[Ni(ddpd)_2](BF_4)_2$. *Zeitschrift für Anorganische und Allgemeine Chemie, 644*(14), 706–712. https://doi.org/10.1002/zaac.201800101
201. González, E., Rodrigue-Witchel, A., & Reber, C. (2007). Absorption spectroscopy of octahedral nickel(II) complexes: A case study of interactions between multiple electronic excited states. *Coordination Chemistry Reviews, 251*(3–4), 351–363. https://doi.org/10.1016/j.ccr.2006.08.011
202. Nolet, M.-C., Michaud, A., Bain, C., Zargarian, D., & Reber, C. (2006). Allowed and forbidden d-d transitions in poly(3,5-dimethylpyrazolyl)methane complexes of nickel(II). *Photochemistry and Photobiology, 82*(1), 57–63. https://doi.org/10.1562/2005-06-28-RA-593
203. Dab, C., East, N. R., Förster, C., Heinze, K. & Reber, C. (2022). to be submitted.
204. Oppenheim, J. J., McNicholas, B. J., Miller, J., & Gray, H. B. (2019). Electronic Structure of Tetracyanonickelate(II). *Inorganic Chemistry, 58*(22), 15202–15206. https://doi.org/10.1021/acs.inorgchem.9b02135
205. Giordano, T. J., Butler, W. M., & Rasmussen, P. G. (1978). Platinum and palladium complexes of thienylpyridine. 2. Quasi-octahedral divalent-metal compounds. *Inorganic Chemistry, 17*, 1917–1922.
206. Takeda, N., Shimizu, D., & Tokitoh, N. (2005). Synthesis and structure of a distorted octahedral palladium(II) complex coordinated with a tetrathioether ligand tethered with bulky substituents. *Inorganic Chemistry, 44*(23), 8561–8568. https://doi.org/10.1021/ic050944v
207. Pointillart, F., Train, C., Villain, F., Moulin, C. C. D., Gredin, P., Chamoreau, L.-M., Gruselle, M., Aullon, G., Alvarez, S., & Verdaguer, M. (2007). Six-fold oxygen-coordinated triplet (S = 1) palladium(II) moieties templated by tris(bipyridine) ruthenium(II) ions. *Journal of the American Chemical Society, 129*(5), 1327–1334. https://doi.org/10.1021/ja066817v
208. Takeda, N., Isobe, T., & Tokitoh, N. (2007). Synthesis of an acyclic diselenodithioether ligand tethered with bulky substituents and its application to the synthesis of a distorted octahedral palladium(II) complex. *Heteroatom Chemistry, 18*(5), 549–556. https://doi.org/10.1002/hc.20339
209. Das, D., Vats, B. G., Kannan, S., Maity, D. K., & Drew, M. G. (2013). Steric effects in pyrazole palladium(II) compounds: Synthetic, structural, and theoretical studies of a highly distorted octahedral palladium(II) pyrazole compound. *Polyhedron, 54*, 104–109. https://doi.org/10.1016/j.poly.2013.01.051
210. Safin, D. A., Babashkina, M. G., & Garcia, Y. (2013). First paramagnetic Pd(II) complex with a PdN_4S_2 coordination core. *Dalton Transactions, 42*(4), 902–905. https://doi.org/10.1039/C2DT32505E